

pubs.acs.org/Macromolecules Article

Hybrid Field Theory and Particle Simulation Model of Polyelectrolyte-Surfactant Coacervation

Jason J. Madinya and Charles E. Sing*



Cite This: Macromolecules 2022, 55, 2358-2373



ACCESS I

III Metrics & More

Coacervate 0.01

Article Recommendations

ABSTRACT: Solutions of oppositely charged polyelectrolytes and surfactants have been widely studied for a variety of applications; they play an important role in the formulation of personal care products, can be used as an effective strategy for drug encapsulation, and serve as analogues to biological systems such as biomolecular condensates. Surfactant molecules self-assemble into micellar macroions that are known to form complexes with oppositely charged polyelectrolytes and can undergo a bulk liquid-liquid phase separation known as complex coacervation.

This process results in a "coacervate" phase that is rich in macroions and a "supernatant" phase that is dilute in macroions. It is challenging to model this phase separation process due to the disparate length scales and strong Coulombic interactions in these mixed macroion systems. In this work, we present a hybrid simulation and field theory model to describe polyelectrolyte/surfactant solutions, where the surfactant species has self-assembled into worm-like micelle structures. We use self-consistent field theory (SCFT) to model the polyelectrolytes in the solution which interact with the surfactant micelles. The surfactant micelle structures are determined by performing Monte Carlo (MC) simulations, which are used to determine applied external fields in the SCFT portion of the model. We use these calculations to determine the system free energy and map the phase diagrams for polyelectrolyte-surfactant coacervates and subsequently consider the effect of a number of molecular parameters such as polyelectrolyte chain length, the volume of the interacting micelle surface sites, and the electrostatic binding energy between the polyelectrolyte and micelle surface. Our model shows that local charge—charge correlations are critical for phase separation to occur. Additionally, we evaluate the statistics of micelle bridging by the polyelectrolyte and the relationship between bridging and the densities of the macroions and salt ions. This hybrid SCFT/MC model can be generalized to study a variety of mixed macroion systems and make predictions for phase behavior and molecular structure.

INTRODUCTION

Solutions of oppositely charged polyelectrolytes and surfactants have been studied extensively for a variety of applications, including drug encapsulation, 1-3 personal care products, 4-8 and food products. 9-11 These systems are known to exhibit a number of self-assembly or phase behaviors, driven by a complicated interplay of various intermolecular forces, particularly hydrophobic and electrostatic interactions. 12-17 Hydrophobicity drives the self-assembly of surfactant molecules into micelle structures, 18,19 and both hydrophobic and electrostatic interactions can promote the complexation of the polyelectrolytes with the oppositely charged surfactants. 16,17 In addition to the competition between these interactions, the multicomponent nature of these systems-which consist of the polyelectrolyte, the surfactant molecules, both cation and anionic salt species, and water—gives rise to a number of desirable properties that can be readily tuned. 20-22 Most importantly, phase behavior and self-assembly give rise to rheological properties such as foamability, wettability, and lubrication which are commonly used to engineer the sensorial properties⁸ important for consumer applications (i.e., personal

care and food products). Despite the key industrial role of this class of materials, there remain significant gaps in the community's knowledge of the fundamental physics governing the phase behavior of polyelectrolyte-surfactant mixtures. The solution behavior of these systems is the primary focus of this work, where we present a model for predicting the phase behavior of worm-like surfactant micelles in solution with polyelectrolytes.

Polyelectrolyte-Surfactant Micelle Complexation and Assembly. Most of the current understanding of polyelectrolyte-surfactant mixture phase behavior stems from experimental measurement and typically involves characterizing a number of key quantities that capture the relationship between

Received: January 25, 2022 Revised: February 23, 2022 Published: March 9, 2022





micelle formation, electrostatic complexation, and assembly. 12,23,24 In aqueous surfactant solutions, the critical micelle concentration (CMC) is one such key quantity and is the concentration above which the surfactant molecules selfassemble into micelle structures.²⁴ For charged surfactants in solution with oppositely charged polyelectrolytes, it is known that this is supplanted by a critical aggregate concentration (CAC) required for the surfactants to aggregate into micelle structures. This concentration is lower than the CMC because the interactions between the polyelectrolyte and the surfactant counteract the like-charge repulsive forces due to the aggregation of the surfactant charges. ^{23,25} This results in the surfactants forming aggregates (i.e., complexes) with the polyelectrolytes, which decorate the charged surfaces of the aggregates; these complexes form the foundation for a number of phases and self-assembled structures and represent the major challenge for describing polyelectrolyte—surfactant systems. ^{26,27}

In addition to complexation, polyelectrolyte—surfactant systems above the CAC can self-assemble into structures formed by ordering the surfactant micelles. 26,27 A number of structures have been proposed and measured, including precipitates and gels. 30,31 More standard self-assembled structures, such as lamellar structures, 32 as well as cylindrical micelles and spherical vesicles $^{33-35}$ have been reported, where the polyelectrolyte chains forms a network with the cylindrical micelles or spherical vesicles as the nodes. The spherical vesicle structure with the polyelectrolytes connecting the vesicles is often termed "string of pearls" or "necklace" structure in the literature. $^{33-35}$ Additionally, core—shell structures have also been reported, where there is a critical polymer—surfactant charge ratio Z_o above which the surfactants form a micellar core with the polyelectrolytes decorating the surface of the core. 35,36

Polyelectrolyte—Surfactant Micelle Phase Separation. The key feature of polyelectrolyte—surfactant systems, which is the focus of this work, is the emergence of a bulk phase separation known as *complex coacervation*. Complex coacervation refers to the charge-driven liquid—liquid phase separation phenomenon that occurs in oppositely charged macromolecules. The liquid—liquid phase separation results in the formation of a phase that is rich in macroions, the *coacervate* phase, and a phase that is dilute in macroions, known as the *supernatant*. There has recently been considerable interest in studying coacervation in a variety of different mixed macroion solutions, including surfactant and polyelectrolyte solutions, ^{37–41} as well as other biologically relevant systems such as charged colloids and polyelectrolyte solutions ^{42–46} and charged proteins and polyelectrolytes.

There has been extensive work on characterizing this phenomenon in polyelectrolyte—surfactant systems, though there is still not an agreed-upon physical picture of phase separation and self-assembly in polyelectrolyte—surfactant systems and other mixed macroion solutions. Works by Dubin et al., ⁵² Wang et al., ¹⁴ and Kizilay et al. ⁵³ show that polyelectrolyte—surfactant complexation and coacervation are highly dependent on the linear charge density of the polyelectrolyte, the surface charge density of the surfactant micelle, and the ionic strength of the solution. Wang et al. ¹⁴ suggest that changes in salt concentration can enhance or suppress coacervation due to changes in the binding affinity between the polymer and micelle. These findings suggest that strong electrostatic attractions between the oppositely charged macroions are a driving force in complexation and coacervation.

In this work, we are particularly interested in understanding complex coacervation in solutions of polyelectrolytes and surfactants that have self-assembled into disordered, worm-like surfactant micelles. These micelles are also known to form ordered phases, but for this early stage of model development we restrict our focus to disordered worm-like micelles. We expect that this model can eventually be modified to model coacervation with ordered micelle structures but leave this for future work.

Polyelectrolyte-Polyelectrolyte Coacervation Models. To understand complex coacervation in surfactantpolyelectrolyte solutions, we draw upon the considerable amount of work done on studying coacervation between two oppositely charged polyelectrolytes. 54-76 One of the proposed key mechanisms for coacervation in polyelectrolytes is the phenomenon known as "counterion release", 57 which is characteristic of macroions with high charge densities. 77,78 Counterion release refers to an increase in translational entropy due to the release of condensed salt ions⁷⁷ upon complexation between two oppositely charged macroions;⁷⁸ this and the related concept of ion pairing are invoked in a number of models that are developed to explain a variety of coacervates composed of high linear charge density polyelectrolytes and are used to explain not just standard polyelectrolyte coacervation⁵⁸ but also charge-sequenced polyelectrolytes⁷⁹ as well as self-coacervation in sequenced polyampholytes.⁸⁰ Conversely, low linear charge density polyelectrolytes are thought to form coacervates due to fluctuation-driven attractions, an approach that has also been used to model sequence and polyampholyte effects. 57,68,70,81-83 The relationship between fluctuation-driven and counterion release-based mechanisms, and their role in real polyelectrolyte coacervates, remains an active area of research. In coacervation between polyelectrolytes and oppositely charged surfactant micelles, coacervation may be driven by electrostatic fluctuation forces and/or counterion release; however, the impact of one driving force over the other is thought to depend on the specific macroion species being studied.⁸⁴ Experimental efforts to understand these thermodynamic mechanisms have focused on the strong dependence of phase behavior on both temperature⁸⁵ and polyelectrolyte molecular weight.⁸⁶

Modeling Polyelectrolyte-Surfactant Micelle Coacervation. There have been very few efforts to model mixed macroion coacervates with respect to either ion-piaring or fluctuation-based attraction, despite significant progress in polymeric coacervates. Perhaps the only theoretical or computational effort we are aware of has been the progress made by Ganesan and co-workers to model fluctuation-based attraction between charged colloids in polyelectrolyte solutions. 42-46 They have modeled both uniformly charged colloids 42,46 and patchy colloids^{43–45} and have quantified their attraction in oppositely charged polyelectrolyte solutions. This has served as the input to larger length-scale simulations of coacervation, and they have mapped out some important phase behaviors. Like the linear chain systems, however, fluctuation-driven attraction is typically limited to small concentrations of charged species (i.e., salt, polymer, and micelle). This is because "ion pairing" and other local correlation interactions are not as clearly resolved. In analogy to polyelectrolyte coacervates, 64,87,88' a model to account for ion pairing and other local correlation effects will be necessary to span all polymer and micelle charge densities found in experimental systems.

In this work, we present a field theory model for coacervation in oppositely charged surfactant micelle and polyelectrolyte

solution. Our model assumes that the surfactant concentration is well above the CAC, which can be verified by comparing the surfactant concentration in the supernatant with CAC values reported in the literature. This model incorporates ion pairing ideas developed in our prior work on polyelectrolytepolyelectrolyte coacervation, 58,79,80,89-92 while still resolving the conformational attributes of these polyelectrolyte chains as they bridge and interact with surfactant micelles. To account for these micelles, we use results from Monte Carlo simulations of worm-like micelle structures to determine the external potentials acting upon the polyelectrolytes in solutions. We show that correlation-driven, electrostatic interactions between the polyelectrolyte and surfactant micelle are required to exhibit coacervation in this mixed macroion solution. We map phase behavior in the context of "effective" ternary phase diagrams used in works by Svensson et al. 40,93 Our model is consistent with a number of features present in these phase diagrams; we predict associative coacervate formation in surfactant micelle and polyelectrolyte solutions,³⁹ meaning both macroions separate into the same phase. We also show that the addition of simple salt results in a reduction of the two-phase region, and at a critical concentration of added salt, phase separation no longer occurs. We can explore the effect of a number of molecular parameters, including polyelectrolyte chain length, surface site charge density, and the strength of the electrostatic correlations between micelles. These parameters are related to a number of quantities commonly used to manipulate phase behavior in polyelectrolyte-surfactant complexes, such as surfactant tail length, 94,95 polymer molecular weight, 94,96 polymer backbone hydrophobicity,⁹⁷ and charge density and charge distribution in the polyelectrolyte. 98-100

HYBRID MONTE CARLO AND FIELD THEORY MODEL

Our approach to modeling polyelectrolyte-surfactant micelle coacervation relies on a hybrid approach to capture both the structure of the surfactant micelle components and the conformations of the complexing polyelectrolytes. We consider a system composed of cylindrical surfactant micelles with negatively charged surfaces, positively charged polycations, and small molecule salt ions as shown in Figure 1. Motivated by the "effective" ternary phase diagram schemes used by Svensson et al., 40,93 we consider only charge-neutral complexes, where all charged components are paired with another component of opposite charge. The components include polymer-micelle complexes (with a volume fraction ϕ_{pm}), polymer-salt complexes (ϕ_{ps}) , and the solvent ϕ_{w} . Identifying stoichiometrically coupled pairs of species as components ensures charge neutrality of the overall solution. We note that in this model salt only exists as part of the polymer-salt complex, and thus we only consider the small-molecule anion that is the counterion to the polycation. There are no small-molecule cations included in this approach—a decision that drastically simplifies both the phase diagram and the model and could be relaxed in future work. We note that it is possible to recover the volume fractions of the polymer and micelle components separately:

$$\phi_{pm} = 2\langle \phi_p(\Psi_s = M) \rangle + \phi_m^{\text{interior}}$$
 (1)

$$\phi_{ps} = 2\langle \phi_p(\Psi_s = S) \rangle \tag{2}$$

$$\langle \phi_m^{ss} \rangle = \langle \phi_p(\Psi_s = M) \rangle$$
 (3)

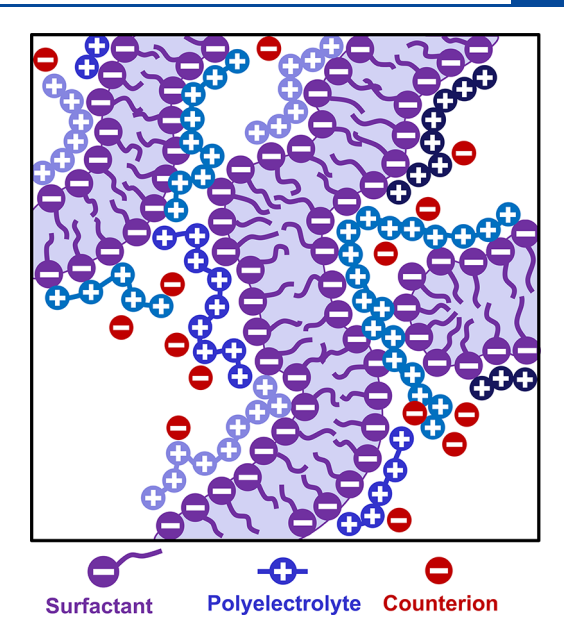


Figure 1. Schematic illustrating the polyelectrolyte and surfactant micelle solution. The polyelectrolyte chains are shown in blue, where different shades represent individual chains. Small ion salt molecules are represented by the red spheres. The surfactant micelles are represented by the purple structures, where the surfactant molecules are the individual sets of heads and tails, and they are organized into a wormlike micelle structure, with the charged heads on the surface of the micelle. The polyelectrolyte chains are shown interacting with and binding to the micelle surfaces, where a single polyelectrolyte chain may be binding with separate micelle structures.

$$\langle \phi_{s} \rangle = \langle \phi_{p}(\Psi_{s} = S) \rangle \tag{4}$$

where ϕ_m^{interior} is the volume fraction of the surfactant micelle that does not include the interacting surface sites, ϕ_m^{ss} is the volume fraction of the interacting micelle surface sites, and $\langle \phi_p(\Psi_s=M) \rangle$ is the solution-averaged polymer concentration for the micelle-bound monomers. We assume the salt and micelle surface sites bind to the monomers in a 1:1 volumetric ratio and that $\langle \phi_p \rangle = \langle \phi_p(\Psi_s=M) \rangle + \langle \phi_p(\Psi_s=S) \rangle$.

For a given set of concentrations ϕ_{pm} , ϕ_{ps} , and ϕ_{w} , we seek a free energy expression that accounts for the microscopic interactions between the polymeric and micellar species. We consider an extension of the transfer matrix approach used in our prior work, 58,80,89-92,101 which accounts for the ion pairing in a polyelectrolyte-polyelectrolyte coacervation to reflect the strong electrostatic interactions between the species. In this model, we similarly consider a constraint that all charged species are paired, such that each charged polyelectrolyte monomer is accompanied by either one or more micelle surface sites or an oppositely charged salt ion. This pairing requirement is the primary way in which electrostatics is included in our model, with long-range Coulombic interactions neglected due to the screening effect of the high concentration of charged species in coacervates. Thus, the chain is treated as sequence of sites that are in one of two adsorption states: $\Psi_s = M$ for micelle-adsorbed segments, and $\Psi_s = S$ for salt-adsorbed segments. Each segment contributes a state-dependent adsorption energy $(\tilde{\varepsilon}_m, \tilde{\varepsilon}_s)$ to the potential energy of the chain, with an additional modification to $\tilde{\varepsilon}_m$ if the monomer is between two adjacent micelle surfaces; this is the second way in which electrostatics is included in our model and is a phenomenological modification that accounts for complicated charge correlation effects. 102,103 Our approach,

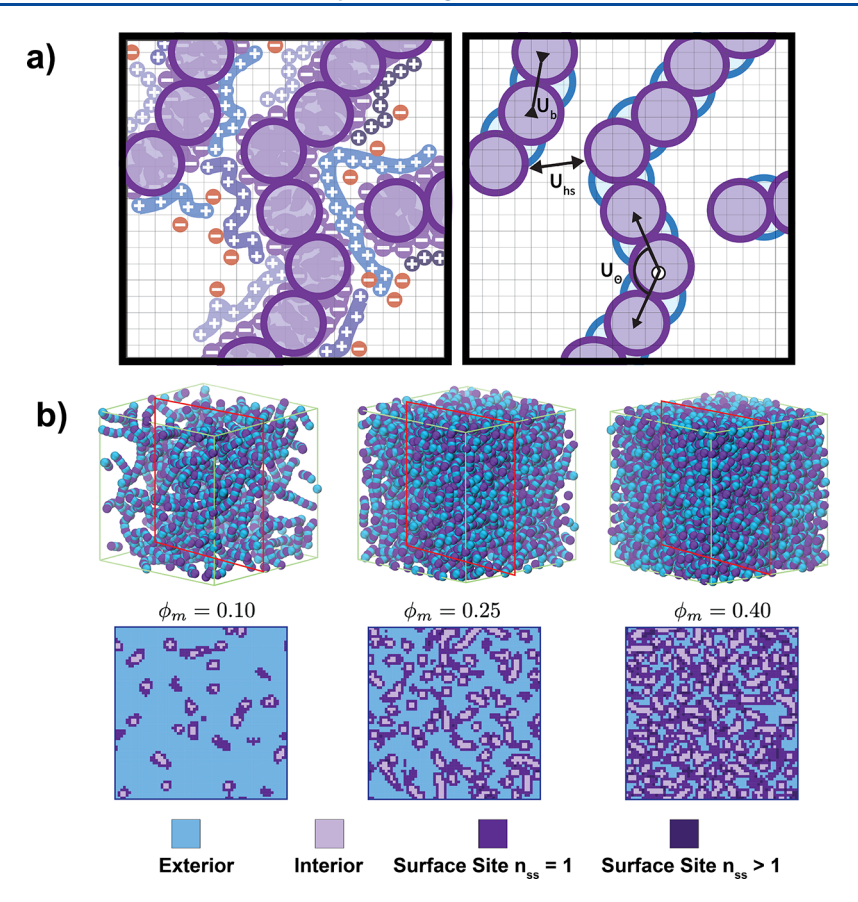


Figure 2. (a, left) We will represent the worm-like surfactant micelles in our model as a chain of beads (purple), where the bead diameter corresponds to the diameter of the surfactant micelle. (a, right) We will run MC simulations on these surfactant micelle beads, incorporating noninteracting interstitial beads (blue) in between the bonded beads (purple) to approximate the cylindrical shape of the micelles. The beads on the chain are connected by a bonded potential U_{bs} and they interact with the other interacting beads through a hard-sphere potential U_{bs} . A bond-angle potential U_{cs} describes the potential tied to the configuration of three consecutive bonded beads. (b) Representative simulation snapshots showing the interacting particles (purple) and the noninteracting interstitial particles (blue). The colormaps below correspond to a slice of the simulation snapshot. The blue areas of the slice correspond to the micelle exterior, the light purple areas correspond to the micelle interiors, and the darker shades of purple correspond to the surface sites, where darker shades represent points with multiple micelle surface sites.

elaborated upon below, considers all possible combinations of adsorption states by incorporating the two states into the calculation of the single-chain partition function in a self-consistent field theory (SCFT) calculation.

SCFT is used to model the conformation of the polyelectrolyte chains, as governed by the inhomogeneous distribution of micelle surface sites and the exclusion of polyelectrolyte and salt from the interior of the micelle structure. This micelle structure will be determined by performing straightforward Monte Carlo (MC) calculations on semiflexible bead-rod chains, which will represent a disordered wormlike micelle structure. Multiple samples of these simulation configurations will be mapped to the field in an SCFT calculation by gridding space and designating each grid as a micelle surface site, micelle interior site, or an unoccupied site (i.e., micelle exterior). The eventual free energy will consist of the free energy from this hybrid MC/SCFT calculation as well as terms related to (1) the mixing entropy of the polymer and salt components and (2) the excluded volume of the polymer and micellar components. We will consider each portion of the calculation in the subsequent section.

Finally, we note that other modeling choices could have been made, for example, by using fluctuating field theories ^{104,105} or integral equation theories ¹⁰⁶ to account for the packing correlations that are an important feature of micelle structures.

These approaches have been successful in modeling mixtures of polymers and larger colloidal structures in other situations and could carry the benefit of modeling these phase-separating systems in a single calculation and formalism. The advantage of our hybrid MC/SCFT approach instead lies in its relatively straightforward implementation, especially in this situation where a simple bead—rod model will be sufficient to resolve the salient structural features of worm-like micelles. This hybrid approach also has the advantage of being versatile, and we anticipate that it can be extended to other types of macroion systems (e.g., proteins or colloids).

Surfactant Micelle Density Field. The SCFT portion of our calculation will rely on having a potential field that accounts for the spatial distribution of the interacting surfactant micelle surface sites as well as the distribution of the surfactant micelle interiors which exclude polymer and salt. The surface site and interior site distributions are predetermined via simulation snapshots of surfactant micelle solutions at various surfactant micelle densities (Figure 2a). We perform these MC simulations using a minimalist model of worm-like micelle structure, described by using the potential βU_m :

$$\beta U_{m} = \beta U_{hs} + \beta U_{b} + \beta U_{\theta} = \sum_{i} \sum_{j>i} \beta u_{hs,ij} + \sum_{i}' \beta u_{b,i,i+1} + \sum_{i}' \beta u_{\theta,i,i+1,i+2}$$
(5)

This potential is written as sums of pairwise contributions, with prime symbols on summations indicating that these potentials are only applied to beads within the same chains, of length N = 50. The first term consists of hard-sphere potential contributions $\beta u_{hs,ij}$ between beads i and j, which prevents overlap of micelle beads within a bead diameter $\sigma_{hs} = 2.0$:

$$\beta u_{hs,ij} = \begin{cases} 0 & r_{ij} \ge \sigma_{hs} \\ \infty & r_{ij} < \sigma_{hs} \end{cases}$$
(6)

Here, r_{ij} is the distance between beads i and j. There is also a pairwise square well bonding potential $\beta u_{b,i,i+1}$ contributing to an overall bonding potential βU_b connecting them into chain structures:

$$\beta u_{b,i,i+1} = \begin{cases} 0 & r_{i,i+1} \le 1.01 \sigma_{hs} \\ \infty & r_{i,i+1} > 1.01 \sigma_{hs} \end{cases}$$
 (7)

We finally include harmonic bond angle potentials $\beta u_{\theta,i,i+1,i+2}$ that contribute to the overall bending potential βU_{theta} :

$$\beta u_{\theta,i,i+1,i+2} = \frac{\kappa_{\theta}}{2} \theta_{i,i+1,i+2}^2 \tag{8}$$

Here, we use a prefactor $\kappa_{\theta}=3.3$ that yields a persistence length consistent with typical values in the literature. The angle $\theta_{i,i+1,i+2}$ is defined between three subsequent beads, i,i+1, and i+2. The overall MC simulations were performed by using the standard Metropolis criteria, where translational moves were accepted with a probability given by $p_{acc}=\min[1,\exp(-\Delta\beta U_m)]$ where $\Delta\beta U_m$ is the change in the micelle potential for a given move.

These MC simulations were ran at hard-sphere volume fractions from $\phi_{hs}=0.01$ to $\phi_{hs}=0.50$, with $\phi_{hs}=n_{hs}\frac{\pi\sigma_{hs}^3}{6}/L^3$, where n_{hs} is the number of hard spheres and L is the box length. The box length is set to $L=17\sigma_{hs}$. Simulations were run for 100 \times 10⁶ MC steps, which is sufficiently long to obtain equilibrium configurations.

Three sample configurations were selected from each of five equilibrated trajectories for every sampled value of ϕ_{hs} , from which we extract the surface site and interior site distributions. To do this, we first add noninteracting spheres between bonded hard spheres to approximate a cylindrical micelle from the hardsphere chains. The simulation box was discretized into $M^3 = 64^3$ collocation points, and each point was evaluated to determine if it resides on the surface of the micelle, the micelle interior, or micelle exterior (Figure 2b). Additionally, collocation points on the micelle surface were evaluated to determine the number of nonconsecutive micelle segments $n_{m,i}$ that were overlapping with the boundaries of the collocation point. Two potential fields are then generated from the discretization of the MC simulation: a micelle interior energetic penalty field $\Omega(\mathbf{r})$ and the adsorption potential field corresponding to micelle-surface adsorbed segments $\tilde{\varepsilon}_m(\mathbf{r})$. Here we write potentials with a tilde to denote normalization by the thermal energy $k_{\rm B}T$. The first potential field is an energetic penalty for placing the polyelectrolyte segment within the interior of the micelle; this field is set to $\Omega(\mathbf{r}) = 10$ for the micelle interior sites and $\Omega(\mathbf{r}) = 0$ elsewhere. The second

potential field contains the contribution to the chain potential for a segment being in the micelle-adsorbed state, and this potential is set to $\tilde{\varepsilon}_m(\mathbf{r}) \to \infty$ for nonsurface sites, $\tilde{\varepsilon}_m(\mathbf{r}) = \tilde{\varepsilon}_{m,0}$ for surface sites where $n_{m,i}=1$, and $\tilde{\varepsilon}_m(\mathbf{r})=2\tilde{\varepsilon}_{m,0}$ for surface sites where $n_{m,i} > 1$. The differentiation between surface sites with different values of $n_{m,i}$ accounts for the possibility that two nearby charged micelle surfaces can induce strong polyelectrolyte-mediated correlation effects, such that there is an energetic benefit for nearby pairs of surfaces. 102,103 In this case, polyelectrolyte charges are thought of as "paired" with two surface charges simultaneously, a simplification that could be relaxed with insight from molecular simulation or more sophisticated models of surface charge correlations. The binding energy for salt-bound monomers is given by $\tilde{\epsilon}_s = \ln(A_0 \phi_s)$, where $A_0 = 20.0$ as used in our previous work. Finally, the solutionaveraged micelle-adsorbed polymer segment density $\phi_{p,m}$, which corresponds to the solution averaged micelle surface site density, can be calculated as follows:

$$\langle \phi_{p,m} \rangle = \sum_{i} n_{m,i} \phi_{ss} \tag{9}$$

where ϕ_{ss} is the local density of a surfactant micelle surface site. The potential fields determined from the MC simulations are used to inform the SCFT, where the partition function of a polyelectrolyte in an environment corresponding to that from the MC simulation can be evaluated.

SCFT Model of Complexing Polyelectrolytes. Selfconsistent field theory (SCFT) will be used to consider the interactions of polyelectrolytes with surfactant micelles and determine the conformational properties of these chains due to the potential fields determined from the MC simulations. The advantage to using SCFT is that it can account for the chain conformations and nonbonded interactions in the system by decoupling the interparticle interactions and considering the system as a polymer density field that interacts with applied and internally generated fields related in this case to the micelle structure. 105 The internally generated field will enforce the constraint of ion binding and set a target monomer density that was determined via the MC simulations described in the previous section. Ultimately, this allows us to evaluate the partition function of the chains and correspondingly the contributions to the free energy of the polyelectrolyte chain.

We model the polyelectrolyte as a Gaussian chain, where the bond length between polymer segments form a Gaussian distribution. The bonding potential of the Gaussian chain can be expressed in the standard way: 105,108

$$\beta U_b[\mathbf{r}] = \frac{3}{2b^2} \sum_{i}^{n_p} \int_0^{N_s} \mathrm{d}s_i \left| \frac{\mathrm{d}\mathbf{r}_i(s_i)}{\mathrm{d}s_i} \right|^2 \tag{10}$$

where b is the segment length, N_s is the number of segments in one chain, n_p is the number of chains in the system, and s corresponds to a coordinate along the chain contour. In addition to this bonded contribution to the system energy, segments along the chain can interact with the small molecule salt ions in the solution as well as the oppositely charged surfactant micelle surface sites. This model considers the limit in which all the segments are paired with either a salt ion or a micelle surface site, and each segment is assigned a state Ψ_s that corresponds to its paired charge ($\Psi_s = S$ and $\Psi_s = M$, respectively). As such, the chain can be treated as a series of adsorption sites that contribute an adsorption energy corresponding to its state, $\tilde{\varepsilon}_s$ and $\tilde{\varepsilon}_m(\mathbf{r})$. Additionally, there is an energetic penalty for a polymer segment

Macromolecules Article pubs.acs.org/Macromolecules

to occupy a space within the surfactant micelle interior. This energetic penalty has been described in the previous section and is denoted as $\hat{\Omega}(\mathbf{r})$. The contribution to the internal energy of the chain from the interactions with the opposite charges as well as the excluded volume of the micelle interior can be expressed

$$\beta U_{nb} = \sum_{i}^{n_{p}} \int_{0}^{N_{s}} ds_{i} [\tilde{\varepsilon}_{m}(\mathbf{r}(s_{i})) \delta(\Psi_{s_{i}} = M) + \tilde{\varepsilon}_{s} \delta(\Psi_{s_{i}} = S) + \Omega(\mathbf{r}(s_{i}))]$$
(11)

Here we have used $\delta(\Psi_{s_i} = X)$ as a way to denote the specific state Ψ of monomer s_{ij} two options X = S, M that must be considered at each grid point in enumerating the single-chain partition function that will be discussed in detail later.

From these potentials, the configurational partition function can be represented as

$$\mathcal{Z}_{c} = \frac{z_{0}^{n_{p}}}{n_{p}!} \prod_{i}^{n_{p}} \sum_{\{\Psi_{s_{i}}\}} \int \mathcal{D}\mathbf{r}_{i} \exp(-\beta(U_{b}[\mathbf{r}^{n_{p}N_{s}}] + U_{nb}[\mathbf{r}^{n_{p}N_{s}}]))$$

$$\tag{12}$$

This particle-based partition function is transformed into a fieldbased partition function by using the particle to field transformation described in Fredrickson et al.'s monograph. 105 To carry out this procedure, we first define the microscopic polymer segment density operator, which corresponds to the micelle-adsorbed polymer segments, as the following:

$$\hat{\rho}_{p,m}(\mathbf{r}) = \sum_{i}^{n_p} \int ds_i \ \delta(\mathbf{r} - \mathbf{r}(s_i)) \ \delta(\Psi_{s_i} = M)$$
(13)

The reason to define this quantity, which reports only the micelle-bound monomers, is to enforce the constraint that these monomers have the same density as the micelle surface site density field $\rho_m(\mathbf{r})$ that was determined from the MC simulation and gridding procedure described earlier so that $\rho_m(\mathbf{r}) = \hat{\rho}_{p,m}$ for all r. We consider a delta functional constraint:

$$\delta[\rho_m - \hat{\rho}_{p,m}] = \int \mathcal{D}\omega_c \exp(i \int d\mathbf{r} \,\omega_c(\mathbf{r})[\rho_m(\mathbf{r}) - \hat{\rho}_{p,m}(\mathbf{r})])$$
(14)

Here we have written the delta functional as a functional integral over an auxiliary constraining field ω_{ϕ} an expression that can be directly incorporated into the partition function:

$$\mathcal{Z}_{c} = \frac{z_{0}^{n_{p}}}{n_{p}!} \int \mathcal{D}\rho_{m} \int \mathcal{D}\omega_{c} \prod_{i}^{n_{p}} \int \mathcal{D}\mathbf{r}_{i} \sum_{\mathbf{\Psi}_{i}} \exp\left(-\beta U_{b} + i \int d\mathbf{r}\right) \\
\omega_{c}(\rho_{m} - \hat{\rho}_{p,m}) \exp\left(-\sum_{i}^{n_{p}} \int_{0}^{N_{s}} ds_{i} \left[\tilde{\varepsilon}_{m}(\mathbf{r}(s_{i})) \delta(\mathbf{\Psi}_{s_{i}} = M)\right] \\
+ \tilde{\varepsilon}_{s} \delta(\mathbf{\Psi}_{s_{i}} = S) + \Omega(\mathbf{r}(s_{i})) \right] \tag{15}$$

We combine all of the chain-specific terms in the exponential term of the partition function into a single-chain partition function $Q[i\omega_c]$, given by

$$Q[i\omega_{c}] = \frac{1}{Z_{0}} \int \mathcal{D}\mathbf{r}_{i} \sum_{\mathbf{\Psi}_{i}} e^{-\beta U_{b}}$$

$$\exp\left(-\int_{0}^{N_{s}} ds_{i} [\{\tilde{\varepsilon}_{m}(\mathbf{r}(s_{i})) + i\omega_{c}(\mathbf{r}(s_{i}))\}\delta(\mathbf{\Psi}_{s_{i}} = M) + \tilde{\varepsilon}_{s}\delta(\mathbf{\Psi}_{s_{i}} = S) + \Omega(\mathbf{r}(s_{i}))]\right)$$

$$(16)$$

The factor Z_0 is the path integral of a free polymer in zero field; this quantity is independent of the density and auxiliary fields, is extensive, and depends on V. It can therefore be expressed as Z_0 = $g_N V$, where g_N is a factor that is thermodynamically unimportant. We have used the identity $-i \int d\mathbf{r} \ \omega \hat{\rho}_{\nu,m} =$ $-i\sum_{i}^{n_p}\int_0^{n_s} ds_i \,\omega_c(\mathbf{r}(s_i))\delta(\Psi_{s_i} = M)$ to include the constraining field directly into the exponential of the single-chain partition function. We can thus write the partition function as

$$\mathcal{Z}_{c} = \frac{z_{0}^{n_{p}}}{n_{p}!} \int \mathcal{D}\rho_{m} \int \mathcal{D}\omega_{c} \exp\left(i \int d\mathbf{r} \,\omega_{c}\rho_{m}\right) [Z_{0}Q[i\omega_{c}]]^{n_{p}}
= \frac{(z_{0}g_{N}V)^{n_{p}}}{n_{p}!} \int \mathcal{D}\rho_{m} \int \mathcal{D}\omega_{c}e^{-\beta\mathcal{H}[\rho_{m},\omega_{c}]}$$
(17)

Here we have defined a Hamiltonian:

$$\mathcal{H}[\rho_m, \, \omega_c] = -i \int d\mathbf{r} \, \omega_c(\mathbf{r}) \rho_m(\mathbf{r}) - n_p \ln \, Q[i\omega_c]$$
(18)

In this model, the micelle surface sites are fixed for a given MC-determined micelle configuration; therefore, the functional integral over ρ_m has only one term and can be left out of the SCFT calculation. In effect, we approximate an integral over this variable by performing this calculation over multiple instances of these micelle configurations for a given micelle and polymer concentration. To solve for the partition function, we invoke a mean-field assumption that there is a single field ω_c^* that minimizes the Hamiltonian $\mathcal{H}[\omega_{\!\scriptscriptstyle c}^*]$ and that this field dominates the path integral over $\omega_{\rm c}$ of the partition function. Therefore, we can approximate Z_c as

$$\mathcal{Z}_{c} \approx \frac{(z_{0}g_{N}V)^{n_{p}}}{n_{p}!} \exp(-\mathcal{H}[\omega_{c}^{*}])$$
(19)

This allows direct calculation of the mean-field free energy $\mathcal{F}_{SCFT} = k_B T \ln \mathcal{Z}_c$ for the polyelectrolyte portion of the calculation but first requires determination of the extremized Hamiltonian $\mathcal{H}[\omega_c^*]$ via a numerical SCFT calculation.

Numerical Solution to SCFT. The practical determination of the extremized Hamiltonian $\mathcal{H}[\omega_{\epsilon}^*]$ follows the standard SCFT approach. This requires numerical determination of the single-chain partition function via calculation of the single-chain propagator in the constraining field $i\omega_c(\mathbf{r})$, in conjunction with calculating the density field of micelle-bound monomers $\hat{
ho}_{p,m}$ that is used to determine the magnitude of the same constraining field.

The propagator function $q(\mathbf{r}, s, \Psi_s; [i\omega_c])$ accounts for the Boltzmann weight of a polymer segment from the start of the chain until a defined index s, state Ψ_s , and location \mathbf{r} in a field $i\omega_c(\mathbf{r})$. This allows for a recursive evaluation for the partition function of the whole chain via a Markov process, with the propagator is defined as

$$q(\mathbf{r}, s + \Delta s, \Psi_s; [i\omega_c]) = \int d\mathbf{r}' \sum_{\Psi_s'} \Phi(\mathbf{r}, \Psi_s | \mathbf{r}', \Psi_{s'})$$

$$q(\mathbf{r}', s, \Psi_{s'}' [i\omega_c])$$
(20)

where $\Phi(\mathbf{r}, \Psi_s | \mathbf{r}', \Psi_{s'})$ is the transition weight for a displacement from \mathbf{r} to \mathbf{r}' for the chain segment spanning s to $s' = s + \Delta s$, where s and s' are in states Ψ_s and $\Psi_{s'}$, respectively. This transition probability density can be separated into a diffusive component (\mathbf{r} dependent, $\Phi_{\mathbf{r}}$) and a potential field component (Ψ_s dependent, Φ_{Ψ}):

$$q(\mathbf{r}, s + \Delta s, \Psi_{s'}, [i\omega_{c}]) = \sum_{\Psi_{s'}} \Phi_{\Psi}(\Psi_{s}|\Psi_{s'})$$

$$\int d\mathbf{r}' \, \Phi_{\mathbf{r}}(\mathbf{r}|\mathbf{r}') q(\mathbf{r}', s, \Psi_{s'}, [i\omega_{c}])$$
(21)

We can numerically evaluate this Chapman–Kolmogorov expression through a two-step procedure; first, the integral $\int d\mathbf{r}' \, \Phi_{\mathbf{r}}(\mathbf{r}|\mathbf{r}') \, q(\mathbf{r}',s,\Psi_s',[i\omega_c])$ can be calculated by numerically integrating the diffusive portion of the propagator for a Gaussian chain over a segment of length Δs :

$$\frac{\partial}{\partial s}q(\mathbf{r},s,\Psi'_{s};[i\omega_{c}]) = \frac{b^{2}}{6}\nabla^{2}q(\mathbf{r},s,\Psi'_{s};[i\omega_{c}])$$
(22)

We refer readers to the monograph by Fredrickson et al. ¹⁰⁵ for methods to perform this standard numerical calculation; we use a pseudospectral method to evaluate this portion of the propagator. The second step is to evaluate the energetic contribution, which enters via the matrix $\Phi_{\Psi}(\Psi_s|\Psi_{s'})$ of Boltzmann factors related to two adjacent adsorption states Ψ_s and $\Psi_{s'}$. While in principle this matrix could account for interactions between adjacent monomers, as is done in our prior work, ^{58,80,89–92,101} we choose a simple noninteracting form for this matrix:

$$\Phi_{\Psi}(\Psi_{s}|\Psi_{s}) = \begin{cases}
e^{-(\tilde{\varepsilon}_{s} + \Omega(\mathbf{r}))} & \Psi_{s} = S \\
e^{-(i\omega_{c}(\mathbf{r}) + \tilde{\varepsilon}_{m} + \Omega(\mathbf{r}))} & \Psi_{s} = M
\end{cases}$$
(23)

These two steps can be used to integrate from an initial condition $q(\mathbf{r}, s = 0, \Psi_s; [i\omega_c]) = 1$ to obtain the single-chain partition function Q that is given by

$$Q[i\omega_c] = V^{-1} \sum_{\Psi_N} \int d\mathbf{r} \ q(\mathbf{r}, s = N, \Psi_N; [i\omega_c])$$
(24)

Solving for the propagator along the chain is the most computationally costly calculation of our model, as the MC simulation of the surfactant micelle solution was discretized into $M^3 = 64^3$ collocation points.

Calculation of the propagator allows for the determination of the micelle density field from the operator $\hat{\rho}_{p,m}$:

$$\hat{\rho}_{p,m}(\mathbf{r}) = -n_p \frac{\delta \ln \mathbb{Q}[i\omega_c]}{i\omega_c(\mathbf{r})}$$

$$= \frac{\langle \phi_p \rangle}{N_p} \frac{\int_{s=0}^{s=N_s} \mathrm{d}s \ q(\mathbf{r}, s, M, [i\omega_c]) q(\mathbf{r}, N_s - s, M, [i\omega_c])}{1/N_g \sum_{\Psi} q(\mathbf{r}, N, \Psi, [i\omega_c])}$$
(25)

The extremization of the Hamiltonian is performed by satisfying the constraint that $\rho_m(\mathbf{r}) = \hat{\rho}_{p,m}(\mathbf{r})$ for all points \mathbf{r} by modifying the auxiliary field $i\omega_c(\mathbf{r})$. Starting with an initial guess for $i\omega_c(\mathbf{r})$, we evaluate the propagator via eq 21 to determine single-chain

partition function in eq 24. This can be used to calculate the density operator via eq 25. Comparison of this density operator, which represents the density of micelle-bound monomers, with the density of micelle surface sites informs the update of the constraining field:

$$i\omega_{c}(\mathbf{r}) = i\omega_{c}(\mathbf{r})' - \alpha \frac{\delta H[\omega]}{i\delta\omega_{c}(\mathbf{r})} = i\omega_{c}(\mathbf{r})' - \alpha(\rho_{m}(\mathbf{r}) - \hat{\rho}_{p,m}(\mathbf{r}))$$
(26)

Here, the parameter α controls the rate at which the difference of the two density fields converge by setting the per-iteration correction to the constraining field, which is chosen to converge as quick as possible while still maintaining numerical stability.

Solution Free Energy. The iterative SCFT calculation obtains an auxiliary constraining field $i\omega_c^*(\mathbf{r})$ that extremizes \mathcal{H} , allowing us to define a free energy from eq 19 via the relationship

$$\beta \mathcal{F}_{\text{SCFT}}/V = \frac{1}{V} \ln \mathcal{Z}_c = -\frac{n_p}{V} \ln(z_0 g_N V) + \frac{n_p}{V} \ln n_p - \mathcal{H}[i\omega_c^*(\mathbf{r})]$$
(27)

Assuming a reference volume ν_p for the monomer, we can write the corresponding free energy in terms of the numerical grid system (i.e., over the M^3 collocation points):

$$\frac{\nu_{p}\beta F_{\text{SCFT}}}{V}(\phi_{\text{pm}}, \phi_{\text{ps}}) = \frac{\nu_{p}\beta}{V}F_{0} + \frac{\phi_{p}}{N_{p}}\ln\phi_{p} - i\frac{1}{M^{3}}\sum_{i}^{M^{3}}\omega_{c,i}\phi_{p_{m},i} - \frac{\phi_{p}}{N_{p}}\ln Q[i\omega_{c}]$$
(28)

Here, $\phi_{p_{m}i}$ corresponds to the micelle adsorbed monomer volume fractions, and we use a subscript for $\omega_{c,i}$ and $\phi_{p_{m}i}$ to denote that these are quantities located at discrete grid points i. We also include an arbitrary reference free energy F_0 that is thermodynamically irrelevant but comes from both other constants in the partition function and the conversion to volume fractions ϕ_p . Again, ϕ_{pm} and ϕ_{ps} are the polymer—micelle and polymer—salt complex volume fractions, which can be directly related to the actual values used in the expression (ϕ_p, ϕ_s, ϕ_m) due to electroneutrality.

This result from the SCFT calculation only includes the contribution due to the free energy of the polymeric species, particularly (1) their interactions with surrounding species, (2) their conformational degrees of freedom, and (3) their translational entropy. We also include a number of other terms to account for other interactions not included in this calculation:

- We must include the salt translational entropy, which is the standard expression $\nu_p \beta F_{s,\text{trans}}/V = \phi_s \ln \phi_s$.
- In connection with our previous work on polyelectrolyte-polyelectrolyte coacervation theories, ⁸⁰ we include a phenomenological cubic term to account for excluded volume of the polymer-salt complex:

$$\frac{\nu_{p}\beta F_{ps,\text{ev}}}{V} = \xi \left[\frac{\phi_{ps}}{(1.0 - \langle \phi_{p,m} \rangle - \phi_{m}^{\text{interior}})} \right]^{3}$$
(29)

We note that the denominator reflects the occupation of volume by the micellar components, which contributes to an increase in the effective concentration of the polymeric species. We choose $\xi = 20.0$, which is similar to the value used in our previous work. 58,80,89,91,92 It would in

principle be possible to include a similar term directly in the SCFT portion of the calculation, though we do not consider this complication as we do not expect it to significantly improve the physical meaning of the model.

 We approximate the excluded volume contribution from the surfactant micelle chains using the Carnahan—Starling equation of state¹⁰⁹

$$\frac{\nu_p \beta F_{cs}}{V}(\phi_m') = \frac{\nu_m}{\nu_p} \frac{{\phi_m'}}{\nu_m} \frac{4{\phi_m'} - 3{\phi_m'}^2}{(1 - {\phi_m'})^2}$$
(30)

where ν_m is the volume of the micelle hard-sphere particle from the MC simulations and ϕ'_m is the volume fraction of the micelle chain including the noninteracting interstitial particles and the hard-sphere chain particles from the MC simulations.

These terms accounting for the excluded volume of the surfactant micelle as well as the polymer—salt concentrations are explicitly intended to be non-pairwise interactions. This leads to an overall expression for the free energy of the system, $\mathcal F$

$$\begin{split} \frac{\nu_{p}\beta\mathcal{F}}{V} &= \frac{\nu_{p}\beta}{V} (F_{\text{SCFT}} + F_{s,\text{trans}} + F_{ps,ev} + \beta F_{cs}) \\ &= \frac{\nu_{p}\beta}{V} F_{0} + \frac{\phi_{p}}{N_{p}} \ln \phi_{p} + \phi_{s} \ln \phi_{s} - i \frac{1}{M^{3}} \sum_{i}^{M^{3}} \omega_{c,i} \phi_{p_{m},i} \\ &- \frac{\phi_{p}}{N_{p}} \ln Q[i\omega_{c}] + \xi \left[\frac{\phi_{ps}}{(1.0 - \langle \phi_{p,m} \rangle - \phi_{m}^{\text{interior}})} \right]^{3} \\ &+ \frac{\nu_{m}}{\nu_{p}} \frac{\phi_{m}'}{\nu_{m}} \frac{4\phi_{m}' - 3\phi_{m}'^{2}}{(1 - \phi_{m}')^{2}} \end{split}$$
(31)

This free energy expression will be used to map out the phase behavior of coacervation in polyelectrolyte-micelle systems, and we note that it implicitly includes both the MC simulation results and SCFT calculations in the determination of the constraining field ω_c and the single-chain partition function Q. These thus include key assumptions that will limit the scope of our predictions; first, while we take an ensemble of MC simulations as the foundation for the SCFT, we are limited by the numerical averaging over stochastically determined micelle structures. Importantly, these structures are also not themselves affected by the polyelectrolyte interactions, which is a major assumption that we make in our work. We justify this lack of selfconsistency by noting that the dense branch of the coacervate phase separation is almost always highly packed (ca. $\phi_m \approx 0.5$), and the polyelectrolyte-induced attraction would likely only perturb this structure slightly. Indeed, strong perturbations would likely induce ordering in the micellar structures, a situation we explicitly neglect in this simplified theory. Even in the dilute branch of the coacervate phase separation (i.e., the supernatant) will have a relatively high concentration of micelles (ca. $\phi_m \approx 0.1-0.3$), so again we a posteriori justify our assumption that this lack of self-consistency is not a major deficiency of this model.

Another major assumption is in the nature of the polyelectrolyte interactions, which are treated as pairwise "ion binding" events that come with binding energies $\tilde{\varepsilon}_m$ and $\tilde{\varepsilon}_s$ that must be parametrized. We treat these as tunable parameters and note (1) they can be ostensibly determined from simulation, as

has been done in our prior work, ^{58,80,89,110} where (2) this approach has been used to great effect in describing a number of experimentally validated aspects of coacervation (e.g., sequence, ⁷⁹ branching, ^{89,110} polyampholyte self-coacervation, ⁸⁰ and multivalent ions ⁸⁹). Finally, we note that we invoke the traditional mean-field approximation for the SCFT portion of the calculation. This may be relaxed with more advanced field theoretic calculations ¹⁰⁵ but expect only quantitative improvements that would be small compared to the other approximations we are making. These approximations represent opportunities to further refine this model, which we will save for future efforts.

RESULTS

Free Energy Landscape. The simulation informed, selfconsistent field theory model developed in this paper allows us to determine the system free energy \mathcal{F} for a worm-like surfactant micelle and polyelectrolyte solution. Solution behavior of the system can be determined from the free energy manifold evaluated under a number of key system variables; we will focus on phase behavior as a function of the polymermicelle complex concentration ϕ_{pm} and the polymer-salt complex concentrations ϕ_{ps} , which are the main compositional variables in our model. There are also a number of molecular parameters that can be set within the model and reflect the values that would be determined by the specific species considered. For example, we define the ratio of the ideal radius of gyration of the polymer and the micelle radius, $\Theta = R_o/R_m$, to quantify the difference in length scales between the MC simulations and the field theory. The dependence of R_{σ} = $N_v^{1/2}b/\sqrt{6}$ on Θ links this parameter to the degree of polymerization of the polyelectrolyte, N_v , as well as the segment size of the polyelectrolyte, b. Another tunable molecular parameter in the model is the concentration of the surfactant micelle surface site, ϕ_{ss} . This parameter sets the volume of the surface site, and it is assumed that polyelectrolyte monomers and micelle surface site interact with each other in a 1:1 volumetric ratio. Therefore, the parameter ϕ_{ss} determines how much polymer interacts with each micelle surface site. The quantitative choice for ϕ_{ss} will reflect both the surface charge density of the micelle and the discretization length scale, and so we treat it as a tunable parameter in this model that can be varied to understand its role in coacervate phase behavior. Finally, we tune the strength of interaction between the oppositely charged polyelectrolyte and micelle surface sites via the binding energy for micelle-adsorbed monomers, $\tilde{\varepsilon}_{m,0}$. This parameter not only accounts for both the bare binding energy between the two species but also accounts for correlation-driven attractions between nearby surfaces that in our model are included via the factor of 2 when two or more micelles share a surface site. While the exact nature of this correlation could be refined with molecular simulation 102 or field theoretic arguments, 103 our model keeps this at the level of a phenomenological parameter by virtue of the magnitude of $\tilde{\epsilon}_{m,0}$. Our quantitative choice for this parameter reflects the typical $\approx k_{\rm B}T$ interaction between hydrated charges, accounting for the multiple Coulombic interactions between a polyelectrolyte charge and several charges on the micellar surface. In this paper, we choose a fixed value of $\Theta = 0.4$ for a degree of polymerization of $N_p = 50$ and scale Θ accordingly for different values for the degree of polymerization to maintain the same polymer segment size b. The molecular parameters being tuned, $N_p = 50$, $\tilde{\varepsilon}_{m,0} = -3.50$, and $\phi_{ss} = 0.03$, are held constant unless otherwise indicated.

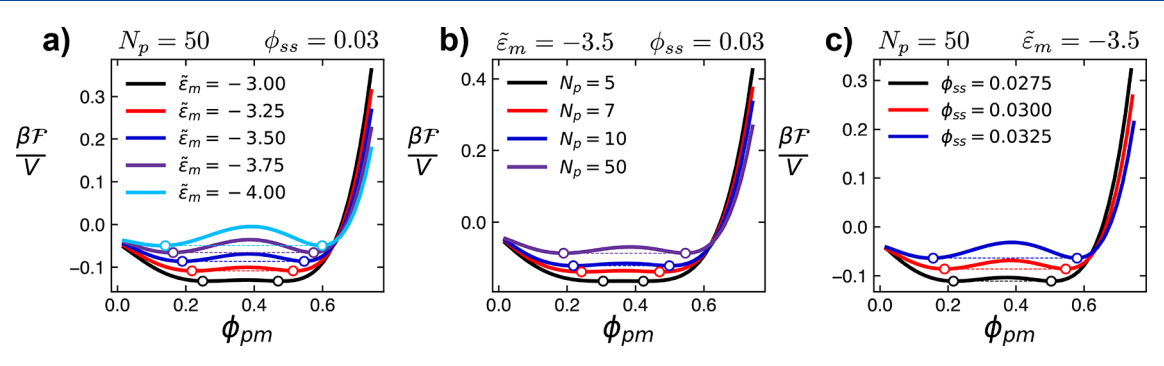


Figure 3. Plots of the free energy density vs polymer—micelle complex concentration while varying (a) micelle binding energy $\tilde{\epsilon}_m$, (b) degree of polymerization N_p , and (c) surface site volume fraction ϕ_s . A linear shift factor of $a \times \phi_{\rm pm}$ is added to the free energy density, with prefactor a chosen such that the common tangents along the curve have approximately equal values for the free energy density. The common tangents are connected by a dotted line.

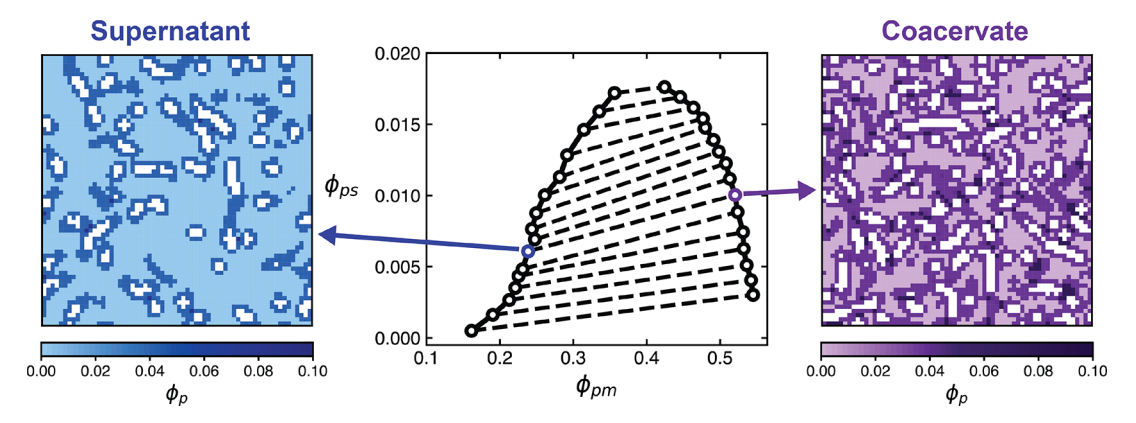


Figure 4. Phase diagram (center) for a polyelectrolyte–surfactant system, in the polymer–salt complex volume fraction ϕ_{ps} vs polymer–micelle complex volume fraction ϕ_{pm} plane. The phase diagram is flanked on each site by a density map of the polymer concentration ϕ_p (see legends) in a 2D slice of the simulation space for the indicated supernatant (blue) composition and corresponding coacervate (purple) composition. The phase diagram shows the binodal for the system with the degree of polymerization $N_p = 50$, micelle binding energy set $\tilde{\epsilon}_m = -3.5$, and surface site volume fraction $\phi_{ss} = 0.03$. The tie lines connect the two compositions in phase coexistence.

These parameters were varied to quantify their effects on the phase separation behavior of the system.

In the limiting case where the solution-average polymer concentration is equal to the solution-average micelle surface site concentration, all of the monomers will be in the micelle-adsorbed state; therefore, $\phi_{ps} = 0$. In this zero polymer—salt complex limit, the free energy can be expressed in terms of only the polymer—micelle complex concentration. The manifold in this limit will therefore be one-dimensional, and the binodal will be the common-tangent points ϕ_{pm}^A and ϕ_{pm}^B , where

$$\left(\frac{\mathrm{d}(\beta\mathcal{F}/V)}{\mathrm{d}\phi_{pm}}\right)_{\phi_{pm}=\phi_{pm}^A} = \left(\frac{\mathrm{d}(\beta\mathcal{F}/V)}{\mathrm{d}\phi_{pm}}\right)_{\phi_{pm}=\phi_{pm}^B}$$

The common tangent points are the coexisting compositions in the two-phase solution (with the phases denoted as A and B). Figure 3 shows the system free energy as a function of ϕ_{pm} with $\phi_{ps}=0$ while comparing the model parameters N_p , $\tilde{\varepsilon}_m$, and ϕ_{ss} . To better visualize the common tangents of the free energy, a thermodynamically irrelevant term linear in polymer—micelle complex concentration was added to the free energy, $a\times\phi_{pm}$. Values for a where chosen such that the free energy density at the two common tangent points are approximately equal so that it is easier to visualize the common tangents, shown in the circular markers. Figure 3A shows the free energy density curve for different values for the micelle-surface binding energy $\tilde{\varepsilon}_m$,

with Θ = 0.4, N_p = 50, and ϕ_{ss} = 0.03. The supernatant polymer micelle complex concentration decreases with decreasing $\tilde{\epsilon}_m$ and the coacervate polymer-micelle complex concentration increases with decreasing $\tilde{\epsilon}_m$. Decreasing the magnitude of the micelle surface binding energy leads to a shrinking of the coexistence concentrations where polymer-micelle complexes undergo macroscopic phase separation, illustrating that strong correlation interactions are necessary to observe the formation of polymer-micelle coacervates. Figure 3B shows the free energy density curves for different degrees of polymerization for the polyelectrolyte N_p , and the other model parameters are set to $\tilde{\varepsilon}_m = -3.5$ and $\phi_{ss} = 0.03$. For $N_p = 50$, the ratio of the radius of gyration of the polyelectrolyte to the surfactant micelle radius is set to $\Theta = 0.4$. Θ is scaled for the other values of N_p to maintain a consistent segment size, $\Theta' = \Theta_{\gamma} N_p'/N_p$. The change in $\beta \mathcal{F}/V$ vs ϕ_{pm} between the degree of polymerization values of N_p = 10 to $N_v = 50$ is small given the large change in chain length, with only minor changes to the common tangent locations that result in a slight increase in the coexistence region. Conversely, a decrease of the degree of polymerization from $N_p = 10$ to $N_p = 5$ significantly shifts the common tangent points, so that the window for phase separation becomes significantly diminished. In the low N_p limit, the polymer translational entropy dominates the free energy and favors mixing; however, as N_p is increased, this term becomes negligible. This is similar to what is seen to occur in polyelectrolyte-polyelectrolyte coacervates, which

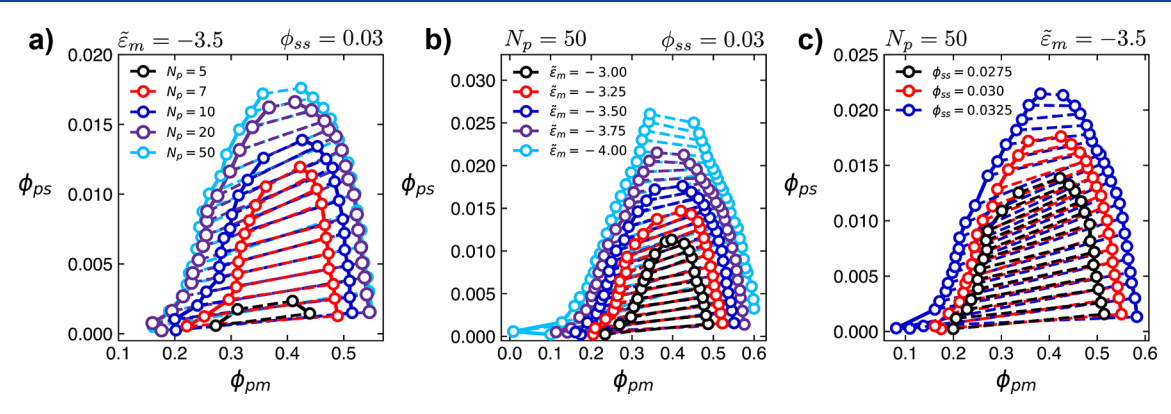


Figure 5. Plots comparing the ϕ_{ps} vs ϕ_{pm} phase diagrams for different values of (a) degree of polymerization N_p , (b) micelle binding energy $\tilde{\varepsilon}_{mp}$ and (c) surface site volume fraction ϕ_{ss} . The parameters not being varied in each plot are held constant to the following values: $N_p = 50$, $\tilde{\varepsilon}_m = -3.5$, and $\phi_{ss} = 0.03$.

exhibit phase diagrams that become essentially insensitive to the degree of polymerization at sufficiently high chain lengths. 63,111 Figure 3C shows the free energy density curves for different values for ϕ_{ss} . The degree of polymerization is set to $N_p=50$, and the micelle-surface binding is set to $\tilde{\epsilon}_m=-3.5$. As the surface site volume fraction ϕ_{ss} is increased, the amount of polymer each surface site can bind is increased; therefore, the free energy stabilization as a result of attractive polyelectrolyte—micelle interaction is enhanced. This increase in polymer—micelle interactions can stabilize coacervate phases with higher macroion densities. As the surface site volume fraction is increased, the coacervate phase macroion densities in Figure 3C are increased as indicated by the common-tangent points; the surfactant phase macroion volume fractions correspondingly are decreased with increasing surface site volume fraction.

In the case where the solution-average polymer concentration $\langle \phi_n \rangle$ is greater than the solution-average micelle surface site density $\langle \phi_{ss} \rangle$, the micelle surface sites will still be completely occupied by polymer while the remaining polymer will complex with oppositely charged salt ions. The free energy density manifold will be a surface, and therefore the binodal will be represented by a curve in ϕ_{ps} vs ϕ_{pm} space. The binodal of the free energy manifold is numerically evaluated and plotted in Figure 4 for $N_p = 50$, $\tilde{\epsilon}_m = -3.5$, and $\phi_{ss} = 0.03$. The area below and between the coexistence curves is a two-phase coexistence area, while the area above and outside the coexistence curves is the single-phase region. Dashed tie lines connect the two coexisting phase concentrations, characterized by micelle-dilute (i.e., supernatant) and micelle-concentrated (i.e., coacervate) phases. Increasing the solution-average polymer-salt concentration ϕ_{ns} in a phase-separated solution monotonically decreases the difference between $\phi_{
m pm}$ in the coexisting phases, up to a critical polymer-salt complex concentration. Because of the use of MC simulations to determine representative micelle structures for the SCFT calculation, we can plot example polymer-micelle complex density fields as shown in Figure 4. This figure plots slices of the density fields for the coexisting supernatant and coacervate phases selected in purple and blue, respectively. The polymer chains are localized onto the micelle surface and are excluded from the micelle interiors and thus outline the wormlike micelle structure. Surface sites in contact with more than one surfactant micelle are able bind more polymer, and thus these sites are higher in polymer-micelle complex concentration than the rest of the micelle surface sites. We can see from the density field slices that there are considerably more of these higher density sites in the coacervate

phase than in the supernatant, which drives the formation of the micelle-dense phase; however, we note that these favorable interactions are necessarily dilute compared to a polyelectrolyte-polyelectrolyte coacervate by virtue of the large size of the micelles. Furthermore, the large size of the micelles also prevents them from being partitioned exclusively to the coacervate due to significant excluded volume repulsions. This balance of dilute attractions and excluded volume repulsions is reflected in the relatively small difference in the $\phi_{\it pm}$ concentration between the phases, where both phases have a significant number of micelles. This contrasts with the analogous phase diagrams in polyelectrolyte-polyelectrolyte coacervates, where there are 10 orders of magnitude in difference between the polyelectrolyte concentrations in the supernatant vs the coacervate phases. 63,64,70,111,112 In the low ϕ_{ps} limit, the supernatant polymer–micelle concentration is $\phi_{pm} \approx 0.15$, with the micelle component occupying most of that volume. This is several orders of magnitude higher than the submillimolar (1 mM DTAB is approximately $\phi_{\rm pm} \approx 2.6 \times 10^{-4})$ critical aggregate concentrations reported in the literature for a typically studied polyelectrolyte and oppositely charged surfactant mixture. 23,113

Figure 5 compares the phase diagrams for different values for the model parameters N_p , $\tilde{\varepsilon}_m$, and ϕ_{ss} . Figure 5A shows the two phase coexistence curves for different values for the degree of polymerization, from $N_p=5$ to $N_p=50$. The micelle binding energy is set to $\tilde{\varepsilon}_m=-3.5$, and the surface site concentration is set to $\phi_{ss}=0.03$. The minimum value for N_p that shows phase separation is $N_p=5$. Lowering the degree of polymerization further increases the free energy density contribution from the polymer translational entropy which stabilizes the single phase solution. As N_p is initially increased above $N_p=5$, the two-phase region expands significantly. However, above $N_p\approx 20$, there is very little change as the value of N_p is further increased. This is again attributed to the polymer translational entropy become negligible compared to the other terms in the free energy density.

Figure 5B shows the two-phase coexistence curves for differing values for the micelle binding energy $\tilde{\epsilon}_m$, with a degree of polymerization of $N_p = 50$, and the surface site concentration set to $\phi_{ss} = 0.03$. As the magnitude of $\tilde{\epsilon}_m$ becomes larger (i.e., becomes more negative), the coexistence region increases significantly due to the increased attraction between monomers and the surfactant micelle surface sites. This increased propensity to phase separate is consistent with the idea that phase separation between oppositely charged surfactant micelles and polyelectrolytes is driven by the electrostatic attraction

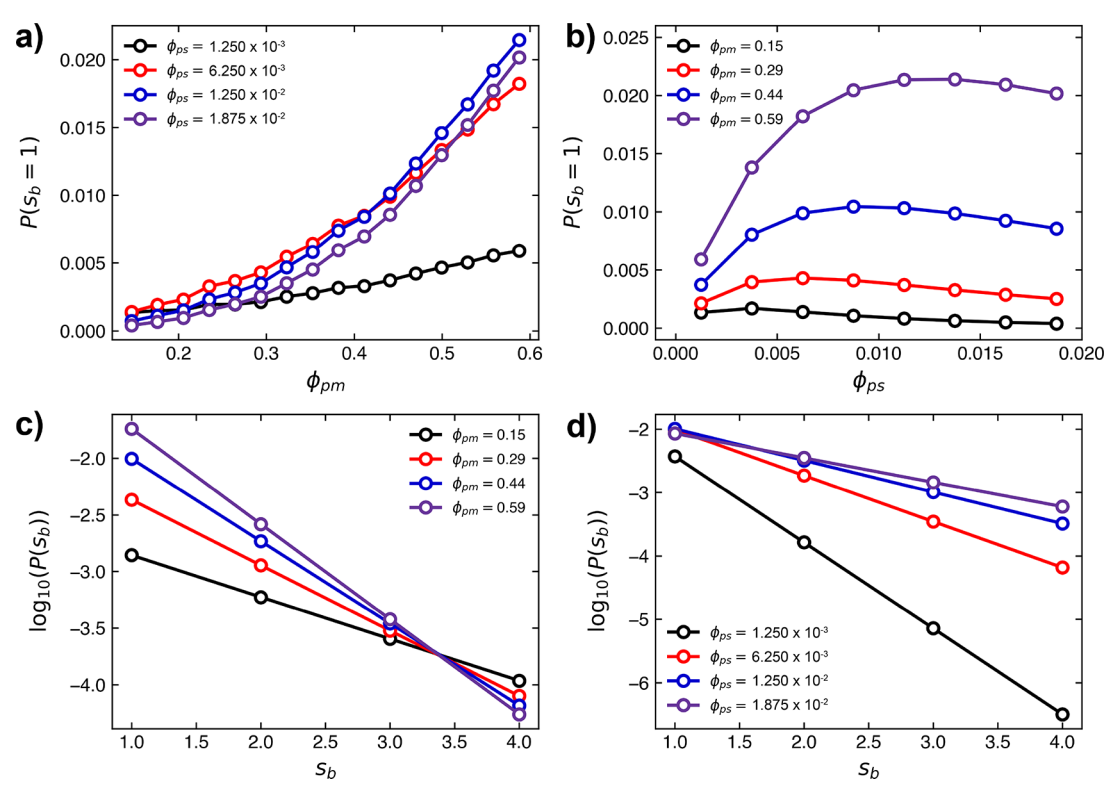


Figure 6. (a) Plot of the bridging probability P for a segment with length $s_b = 1$ vs the polymer—micelle complex concentrations ϕ_{pm} while varying the polymer—salt complex concentration ϕ_{ps} . (b) Plot of the bridging probability P for a segment with length $s_b = 1$ vs the polymer—salt concentration, while varying the polymer—micelle complex concentration. (c) Plot of the logarithm of the bridging probability for a segment length $\log(P(s_b))$ vs the segment length s_b . The polymer—salt complex concentration is held constant at $\phi_{ps} = 6.25 \times 10^{-3}$, and the polymer—micelle complex concentration is varied. (d) Plot of the logarithm of the bridging probability for a segment length $\log(P(s_b))$ vs the segment length s_b . The polymer—micelle complex concentration is held constant at $\phi_{pm} = 0.44$, and the polymer—salt complex concentration is varied.

between the two species; we note that no phase separation is observed if we remove the factor of 2 that multiplies $\tilde{\varepsilon}_{m,0}$ and phenomenologically accounts for correlation-driven attraction between shared (i.e., $n_{m,i} = 2$) surface sites.

Figure 5C shows the phase diagrams for three different values for the surface site volume fraction ϕ_{ss} , with a degree of polymerization of $N_p = 50$ and the micelle binding energy set to $\tilde{\epsilon}_m = -3.5$. As ϕ_{ss} is increased, the two-phase coexistence region is increased, along with the coacervate phase polymer—micelle complex concentration. Similar to $\tilde{\epsilon}_m$, this value tunes the interactions between the polymer and micelle. $\tilde{\epsilon}_m$ changes the strength of attraction between the oppositely charged macroions, and ϕ_{ss} changes the amount of polymer that binds to a micelle surface site. Changes to ϕ_{ss} result in an approximately linear change in the coacervate phase polymer—micelle complex concentration ϕ_{nm} .

Micelle Bridging. Micelle bridging occurs when segments along a polyelectrolyte chain are bound to two distinct micelle assemblies, forming a larger complex. Self-assembly in surfactant and polyelectrolyte solutions have been reported in the literature

to form networks with nodes composed of self-assembled surfactant structures, with polyelectrolytes spanning the surfactant structures. 33-35 The probability that a polyelectrolyte chain will bridge two micelle structures can be evaluated by considering the constrained partition function for the polyelectrolyte chain configurations that span two distinct micelle surface sites, relative to that of the entire set of unspecified chain configurations (i.e., the single-chain partition function Q). Each bridging configuration will have two segments along the chain bound to micelle surface sites, along with some number of salt bound sites s_h in between, giving a total bridging segment length of s_b + 2. Thus, the bridging probability can be described as a function of concentrations ϕ_{ps} and ϕ_{pm} as well as the bridging segment length s_b . We consider intermicelle bridging where the surface sites correspond to beads on distinct hard-sphere chains in the micelle MC simulations as well as intramicelle bridging where the surface sites correspond to nonconsecutive beads on the same hard-sphere chain. The micelle bridging probability can be described as follows:

$$P(\phi_{pm}, \phi_{ps}, s_b) = \sum_{\mathbf{r}} \sum_{\mathbf{r}'} \frac{\sum_{s_0}^{N_s - 2 - s_b} [q(\mathbf{r}, s_0 - 1, M)\tilde{\Phi}(\mathbf{r}, \mathbf{r}', s_b)q(\mathbf{r}', N - s_0 - 1 - s_b, M)]}{\sum_{s_0}^{N_s - 2 - s_b} Q}$$
(32)

Here, s_0 is the location along the chain where the bridging segment begins, \mathbf{r} and \mathbf{r}' are collocation points on the micelle surfaces, and the quantity $\tilde{\Phi}(\mathbf{r},\mathbf{r}',s_b)$ corresponds to the Boltzmann weight of bridging from \mathbf{r} to \mathbf{r}' in s_b steps:

$$\tilde{\Phi}(\mathbf{r}, \mathbf{r}', s_b) = \sum_{\{\mathbf{r}_i\}} \Phi(\mathbf{r}, M | \mathbf{r}_{0}, S) \left[\prod_{i}^{s_b} \Phi(\mathbf{r}_{i-1}, S | \mathbf{r}_{i}, S) \right] \Phi(\mathbf{r}_{s_b}, S | \mathbf{r}, M)$$
(33)

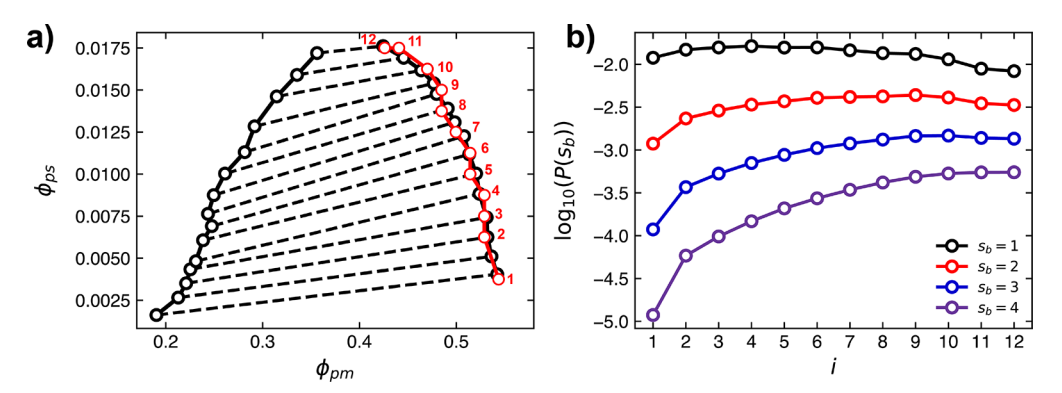


Figure 7. Plots showing a ϕ_{ps} vs ϕ_{pm} phase diagram (a) indicating a set of sampled coacervate-phase compositions (red) i=1-12. Phase diagram corresponds to a solution with $N_p=50$, $\tilde{\epsilon}_m=-3.5$, and $\phi_{ss}=0.03$. (b) Logarithm of the bridging probability for a given bridge segment length $\log(P(s_b))$ at the 12 sampled points i in (a) for a number of different bridge segment lengths s_b .

The summation here is over all $r_i = r_0$, r_1 , ..., r_{s_B} positions of the bridging beads, and the quantities $\Phi(\mathbf{r}_{i-1}, \Psi_{i-1} | \mathbf{r}_i, \Psi_i)$ are once more the transition probability densities described earlier in this paper.

The micelle bridging probability was evaluated for a range of polymer–micelle complex concentrations (0.12 $\leq \phi_{pm} \leq$ 0.6), a range of polymer-salt complex concentrations $(1.25 \times 10^{-3} \le$ $\phi_{ps} \le 1.875 \times 10^{-2}$), and bridging segment lengths $s_b = 1$ to $s_b = 1$ 4. The molecular parameters are $N_p = 50$, $\tilde{\varepsilon}_m = -3.5$, and $\phi_{ss} =$ 0.03. Figure 6a shows the bridging probability with a bridging segment length of $s_b = 1$ as a function of polymer-micelle complex concentration ϕ_{pm} , for varying values for ϕ_{ps} . We initially focus on $s_b = 1$ due to its predominance over $s_b < 1$ (see later) and use it as an overall proxy for the frequency of bridging. The bridging probability for $\phi_{ps} = 1.25 \times 10^{-3}$ is significantly lower than in the higher ϕ_{vs} cases, which we attribute to the lack of available salt ions that are needed to bind the polymer to form the bridge. The bridging probabilities for the three higher $\phi_{\nu s}$ values are similar in magnitude to the low- ϕ_{ps} case in the low- ϕ_{pm} limit; however, they exhibit a significant increase in bridging probability starting around $\phi_{pm} = 0.35$ compared the low- ϕ_{ps} case. This suggests that away from the low- ϕ_{ps} limit the ability for a micelle to bridge is limited by the availability and proximity of micelle surface sites to bridge rather than the availability of salt ions. We justify this by noting that as ϕ_{pm} is increased, the number of collocation points that correspond to a surface site of more than one micelle structure $(n_{ss} < 1)$ is increased. These sites are expected to have the highest probability of bridging as the bridge origin and bridge terminus are located within the same collocation point.

Figure 6b shows the bridging probability for a bridging segment length of $s_b = 1$ as a function of polymer—salt complex concentration ϕ_{ps} , ϕ_{pm} is varied corresponding to the different color plots. For all values of ϕ_{pm} , the bridging probability increases as ϕ_{ps} is increased followed by a subtle decrease as ϕ_{ps} is further increased. The turnover point or the maxima of the plots are shifted toward higher ϕ_{ps} as ϕ_{pm} is increased. These results suggest that once there is sufficient available ϕ_{ps} to draw the polyelectrolyte off the micelle making it available to bridge, the limiting factor becomes the propensity for a bridging polyelectrolyte to terminate after a certain bridging length s_b .

Figures 6c and 6d show the logarithm of the bridging probability as a function of bridging segment length s_b , with varying polymer—micelle complex concentrations (c) and polymer—salt complex concentrations (d). In all cases, the logarithm of the bridging probability is linear with respect to s_b ,

indicating that the vast majority of bridges are $s_b = 1$, justifying our previous use of this value as a proxy for bridging frequency. We expect the quantitative aspects of this trend to be sensitive to physical parameters, such as polymer length and stiffness, but note that the exponential decay of $P(s_b)$ is characteristic of a constant per-monomer probability of bridging vs not bridging. This is observed over a wide range of values of ϕ_{pm} and ϕ_{ps} . Interestingly, in Figure 6c, it is apparent that the relationship between bridging probability and ϕ_{pm} is reversed as s_b is increased from $s_b = 1$ to $s_b = 4$. This implies that higher values of ϕ_{pm} lose more propensity to bridge as s_b is increased than lower values of ϕ_{vm} . This may be due to the fact that while there are more surface-site collocation points at higher ϕ_{vm} that can form more bridges; there are also more available sites near the bridge origin, increasing the probability of terminating the bridge at lower s_h .

Figure 6d shows that for $s_b > 1$ the bridging probability is monotonically increasing with increasing ϕ_{ps} . In the low ϕ_{ps} limit, there is a steep drop in bridging probability as s_b is increased, and as ϕ_{ps} is increased, this drop in bridging probability with increasing s_b becomes less severe. This suggests that in the low ϕ_{ps} limit the bridging is limited by the ability for the polyelectrolyte to come off the micelle to form a bridge origin due to a lack of available salt ions. In the high- ϕ_{ps} region, the bridging probability for at a specific s_b is limited by the propensity for the bridge to terminate at that value of s_b , and higher values of ϕ_{ps} make longer bridges more likely to form.

The connection between micelle bridging and coacervation in polyelectrolyte and surfactant solutions is not well understood, but our model can provide some insights into the behavior of micelle bridging polyelectrolytes in the coacervate phase. In Figure 7a, the phase diagram for a system with parameters N_p = 50, $\tilde{\varepsilon}_m = -3.5$, and $\phi_{ss} = 0.03$ is shown in black. The MC simulation configurations corresponding to the complex concentrations closest to the values of the coacervate binodal are shown in red. The logarithm of the bridging probabilities for these points are shown in Figure 7b, where the x-axis corresponds to the points i along the coacervate binodal in Figure 7a. The points along the binodal are arranged in order of increasing ϕ_{ns} and are numbered 1–12. Figure 7b shows that the bridging probability for $s_h = 1$ is relatively consistent through out the points along the binodal, though there is a slight decrease at large i that we attribute to the decrease in micelle density ϕ_{pm} . The points with lower value of i and therefore lower amounts of ϕ_{vs} have lower bridging probabilities for $s_b < 1$ when compared to higher values of i. This trend persists to higher ϕ_{ps} as s_b is

increased. These results indicate that along the binodal in the direction of increasing ϕ_{ps} the number of short bridges remains relatively constant; however, the propensity for longer bridges to form increases sharply.

Taken as a whole, these micelle bridging results highlight the competition between the availability of salt ions that facilitate longer bridging chains and the prevalence of nearby surface sites on neighboring micelles that can form the other end of the bridge. Bridges are thus more likely to form at high salt and surfactant concentrations; however, the bridge length distribution favors short bridges at high surfactant concentrations when there are more surface sites capable of terminating a bridge.

CONCLUSION

We have developed a field theoretic description for solutions of polyelectrolytes with oppositely charged surfactant micelles. In this model, self-consistent field theory is applied to consider polyelectrolytes in solution with worm-like surfactant micelles, whose structure is determined by using Monte Carlo simulations. The compositional space is reduced by considering the electroneutral complexes formed between the polymer and surfactant micelles as well as the polymer and salt ions. External applied potentials are informed by Monte Carlo simulations such that they correspond with the surfactant micelle structure, including the polymer-binding surface sites and the polymerexcluding micelle interiors. The polyelectrolytes are treated as Gaussian chains, under the influence of these external potentials, where each segment is considered to be in one of two bound states: micelle-bound or salt ion-bound. The partition function for the polyelectrolytes in solution is evaluated numerically, from which free energy landscapes were developed in terms of the complex concentrations.

The free energy landscapes allow us to determine the binodals for the two-phase solutions, and phase diagrams were developed for the solutions with varying molecular parameters. These parameters included the degree of polymerization of the polyelectrolyte, the micelle surface site concentration, and the micelle surface site binding energy. We showed that correlation-driven, electrostatic attraction between the polyelectrolyte and surfactant micelle heavily influence the coacervation behavior of the system. We observed that the extent of coacervation becomes saturated starting around $N_p=20$, and an increase in the coacervate phase macroion density was concomitant with an increase in the surface site volume fraction. Similarly, an increase in the magnitude of the polymer—micelle binding energy leads to a significant increase in the two-phase coexistence region.

This model allows us to consider the probability for having certain polyelectrolyte configurations; of particular interest were configurations that bridged micelle surface sites that are distinct from one another. We determined the probabilities for polyelectrolyte chains to bridge two sites as a function of the bridge length and complex concentrations. The relationship between bridging and the concentrations of the complexes as well as the bridging length is not straightforward, though we found that at the low polymer-salt limit bridging is limited by the ability of the polymer to come off the micelle to start a bridge. We also found that with sufficient polymer-micelle concentration, and higher polymer-salt concentration, longer bridges become more probable. Bridging statistics at the compositions along the coacervate binodals are roughly constant as the compositions are varied, though in the low-polymer-salt limit bridging is suppressed, especially for the longer bridge lengths. While further investigation will be required to elucidate the connections between micelle bridging and coacervation in these systems, our results suggest micelle bridging with short bridges (i.e., small s_b) is a feature of coacervation, and as the critical polymer—salt concentration is approached, the formation of longer bridges may contribute to the transition into a single-phase system. We speculate that it may be possible to enhance or suppress bridging through molecular design of the polyelectrolyte as a way to tune phase behavior or other material properties.

In the development of this model, a few key assumptions were made in the interest of simplifying the model, though in principle many of these assumptions can be relaxed. One primary assumption is that the charges in the system are all paired with the opposite charge—a strong binding limit approximation that is a reasonable starting point for high linear charge density polyelectrolytes and high surface charge density micelles. This simplifies our SCFT model to consider only two states $\Psi = S$, M, though generalization to more states is possible. 101 We also limited our model to include only polymer-salt complexes and polymer-micelle complexes, inspired by the "effective" ternary phase diagram schemes used by Svensson et al. 40,93 One direction for future work would be to extend beyond this limited parameter space to provide predictions for a full five-component system of polycations, polyanions, cations, anions, and solvent. The other key assumption of our model is that the electrostatic binding energy felt by a polymer segment is doubled when it is adjacent to more than one micelle assembly. This is an ad hoc representation of more complicated charge correlation effects that are known to arise in nearby surfaces, 102,103 and molecular predictions for the strength of this effect would be needed to parametrize this model for specific surfactant systems.

A key aspect of our model is the fact that the model incorporates the surfactant micelle structure through external potential fields informed by Monte Carlo simulations. This means that any arbitrary structure can studied; while in this case we considered worm-like micelles, any structure can in principle be realized. This includes self-assembling micelle structures and heterogeneously surface-charged structures such as patchy colloids or charged proteins. The relatively low computational costs of the model and its inherent versatility will allow us to continue to study phase behavior in mixed macroion systems, where the long-ranged electrostatics and the size disparities between the macroions can make traditional methods computationally expensive.

AUTHOR INFORMATION

Corresponding Author

Charles E. Sing — Department of Chemical and Biomolecular Engineering, University of Illinois at Urbana—Champaign, Urbana, Illinois 61820, United States; ◎ orcid.org/0000-0001-7231-2685; Email: cesing@illinois.edu

Author

Jason J. Madinya – Department of Chemical and Biomolecular Engineering, University of Illinois at Urbana–Champaign, Urbana, Illinois 61820, United States

Complete contact information is available at: https://pubs.acs.org/10.1021/acs.macromol.2c00187

Notes

The authors declare no competing financial interest.

ACKNOWLEDGMENTS

This material is based upon work supported by the National Science Foundation Graduate Research Fellowship Program under Grant DGE-1746047. The authors also acknowledge support by the National Science Foundation under Grant DMR-1654158 and the Sloan Minority PhD Program. We thank Dr. Tyler Lytle for providing valuable feedback and insight into this project.

REFERENCES

- (1) Mayya, K. S.; Bhattacharyya, A.; Argillier, J.-F. Microencapsulation by complex coacervation: Influence of surfactant. *Polym. Int.* **2003**, *52*, *644*–*647*.
- (2) Shulevich, Y. V.; Nguyen, T. H.; Tutaev, D. S.; Navrotskii, A. V.; Novakov, I. A. Purification of fat-containing wastewater using polyelectrolyte–surfactant complexes. *Sep. Purif. Technol.* **2013**, *113*, 18–23.
- (3) Singh, M.; Briones, M.; Ott, G.; O'Hagan, D. Cationic microparticles: a potent delivery system for DNA vaccines. *Proc. Natl. Acad. Sci. U. S. A.* **2000**, *97*, 811–816.
- (4) Llamas, S.; Guzman, E.; Ortega, F.; Baghdadli, N.; Cazeneuve, C.; Rubio, R. G.; Luengo, G. S. Adsorption of polyelectrolytes and polyelectrolytes-surfactant mixtures at surfaces: a physico-chemical approach to a cosmetic challenge. *Advances in colloid and interface science* **2015**, 222, 461–487.
- (5) Bradbury, R.; Penfold, J.; Thomas, R. K.; Tucker, I. M.; Petkov, J. T.; Jones, C. Manipulating perfume delivery to the interface using polymer–surfactant interactions. *J. Colloid Interface Sci.* **2016**, 466, 220–226.
- (6) Bali, K.; Varga, Z.; Kardos, A.; Varga, I.; Gilányi, T.; Domján, A.; Wacha, A.; Bóta, A.; Mihály, J.; Mészáros, R. Effect of dilution on the nonequilibrium polyelectrolyte/surfactant association. *Langmuir* **2018**, 34, 14652–14660.
- (7) Kristen, N.; von Klitzing, R. Effect of polyelectrolyte/surfactant combinations on the stability of foam films. *Soft Matter* **2010**, *6*, 849–861.
- (8) Benhur, A. M.; Diaz, J.; Amin, S. Impact of polyelectrolyte-surfactant interactions on the rheology and wet lubrication performance of conditioning shampoo. *International Journal of Cosmetic Science* **2021**, 43, 246–253.
- (9) Bonnaud, M.; Weiss, J.; McClements, D. J. Interaction of a food-grade cationic surfactant (lauric arginate) with food-grade biopolymers (pectin, carrageenan, xanthan, alginate, dextran, and chitosan). *Journal of agricultural and food chemistry* **2010**, 58, 9770–9777.
- (10) Sharipova, A.; Aidarova, S.; Grigoriev, D.; Mutalieva, B.; Madibekova, G.; Tleuova, A.; Miller, R. Polymer–surfactant complexes for microencapsulation of vitamin E and its release. *Colloids Surf., B* **2016**, *137*, 152–157.
- (11) Laquerbe, S.; Carvalho, A.; Schmutz, M.; Poirier, A.; Baccile, N.; Messaoud, G. B. pH-switchable pickering emulsions stabilized by polyelectrolyte-biosurfactant complex coacervate colloids. *J. Colloid Interface Sci.* **2021**, 600, 23–36.
- (12) Thalberg, K.; Lindman, B.; Bergfeldt, K. Phase behavior of systems of polyacrylate and cationic surfactants. *Langmuir* **1991**, *7*, 2893–2898.
- (13) Khan, N.; Brettmann, B. Intermolecular interactions in polyelectrolyte and surfactant complexes in solution. *Polymers* **2019**, 11, 51.
- (14) Wang, Y.; Kimura, K.; Huang, Q.; Dubin, P. L.; Jaeger, W. Effects of salt on polyelectrolyte- micelle coacervation. *Macromolecules* **1999**, 32, 7128–7134.
- (15) Hayakawa, K.; Kwak, J. C. Surfactant-polyelectrolyte interactions. 1. Binding of dodecyltrimethylammonium ions by sodium dextransulfate and sodium poly (styrenesulfonate) in aqueous solution in the presence of sodium chloride. *J. Phys. Chem.* **1982**, *86*, 3866–3870.
- (16) Hayakawa, K.; Kwak, J. C. Study of surfactant-polyelectrolyte interactions. 2. Effect of multivalent counterions on the binding of

- dodecyltrimethylammonium ions by sodium dextran sulfate and sodium poly (styrene sulfonate) in aqueous solution. *J. Phys. Chem.* **1983**, 87, 506–509.
- (17) Malovikova, A.; Hayakawa, K.; Kwak, J. C. Surfactant-polyelectrolyte interactions. 4. Surfactant chain length dependence of the binding of alkylpyridinium cations to dextran sulfate. *J. Phys. Chem.* **1984**, 88, 1930–1933.
- (18) Maibaum, L.; Dinner, A. R.; Chandler, D. Micelle formation and the hydrophobic effect. *J. Phys. Chem. B* **2004**, *108*, 6778–6781.
- (19) López-López, M.; López-Cornejo, P.; Martín, V. I.; Ostos, F. J.; Checa-Rodríguez, C.; Prados-Carvajal, R.; Lebrón, J. A.; Huertas, P.; Moyá, M. L. Importance of hydrophobic interactions in the single-chained cationic surfactant-DNA complexation. *J. Colloid Interface Sci.* **2018**, *521*, 197–205.
- (20) Chronakis, I. S.; Alexandridis, P. Rheological properties of oppositely charged polyelectrolyte- surfactant mixtures: effect of polymer molecular weight and surfactant architecture. *Macromolecules* **2001**, *34*, 5005–5018.
- (21) Pagac, E. S.; Prieve, D. C.; Tilton, R. D. Kinetics and mechanism of cationic surfactant adsorption and coadsorption with cationic polyelectrolytes at the silica- water interface. *Langmuir* **1998**, *14*, 2333—2342.
- (22) Chiappisi, L.; Hoffmann, I.; Gradzielski, M. Complexes of oppositely charged polyelectrolytes and surfactants—recent developments in the field of biologically derived polyelectrolytes. *Soft Matter* **2013**, *9*, 3896–3909.
- (23) Jain, N.; Trabelsi, S.; Guillot, S.; McLoughlin, D.; Langevin, D.; Letellier, P.; Turmine, M. Critical aggregation concentration in mixed solutions of anionic polyelectrolytes and cationic surfactants. *Langmuir* **2004**, *20*, 8496–8503.
- (24) Fuguet, E.; Ràfols, C.; Rosés, M.; Bosch, E. Critical micelle concentration of surfactants in aqueous buffered and unbuffered systems. *Anal. Chim. Acta* **2005**, *548*, 95–100.
- (25) Kogej, K.; Škerjanc, J. Fluorescence and conductivity studies of polyelectrolyte-induced aggregation of alkyltrimethylammonium bromides. *Langmuir* **1999**, *15*, 4251–4258.
- (26) Guillot, S.; McLoughlin, D.; Jain, N.; Delsanti, M.; Langevin, D. Polyelectrolyte—surfactant complexes at interfaces and in bulk. *J. Phys.: Condens. Matter* **2003**, *15*, S219.
- (27) Wallin, T.; Linse, P. Polyelectrolyte-induced micellization of charged surfactants. Calculations based on a self-consistent field lattice model. *Langmuir* **1998**, *14*, 2940–2949.
- (28) Antonietti, M.; Conrad, J.; Thuenemann, A. Polyelectrolyte-surfactant complexes: a new type of solid, mesomorphous material. *Macromolecules* **1994**, *27*, 6007–6011.
- (29) Ober, C. K.; Wegner, G. Polyelectrolyte—Surfactant Complexes in the Solid State: Facile building blocks for self-organizing materials. *Adv. Mater.* **1997**, *9*, 17–31.
- (30) Lapitsky, Y.; Kaler, E. W. Formation of surfactant and polyelectrolyte gel particles in aqueous solutions. *Colloids Surf., A* **2004**, 250, 179–187.
- (31) Lapitsky, Y.; Kaler, E. W. Surfactant and polyelectrolyte gel particles for encapsulation and release of aromatic oils. *Soft Matter* **2006**, *2*, 779–784.
- (32) Bergström, L. M.; Kjellin, U. M.; Claesson, P. M.; Grillo, I. Smallangle neutron scattering study of mixtures of cationic polyelectrolyte and anionic surfactant: Effect of polyelectrolyte charge density. *J. Phys. Chem. B* **2004**, *108*, 1874–1881.
- (33) Gradzielski, M.; Hoffmann, I. Polyelectrolyte-surfactant complexes (PESCs) composed of oppositely charged components. *Curr. Opin. Colloid Interface Sci.* **2018**, 35, 124–141.
- (34) Lam, V. D.; Walker, L. M. A pH-induced transition of Surfactant-polyelectrolyte aggregates from cylindrical to string-of-pearls structure. *Langmuir* **2010**, *26*, 10489–10496.
- (35) Goswami, M.; Borreguero, J. M.; Pincus, P. A.; Sumpter, B. G. Surfactant-mediated polyelectrolyte self-assembly in a polyelectrolyte–surfactant complex. *Macromolecules* **2015**, *48*, 9050–9059.
- (36) Hervé, P.; Destarac, M.; Berret, J.-F.; Lal, J.; Oberdisse, J.; Grillo, I. Novel core-shell structure for colloids made of neutral/polyelec-

- trolyte diblock copolymers and oppositely charged surfactants. EPL (Europhysics Letters) 2002, 58, 912.
- (37) Li, D.; Kelkar, M. S.; Wagner, N. J. Phase behavior and molecular thermodynamics of coacervation in oppositely charged polyelectrolyte/surfactant systems: A cationic polymer JR 400 and anionic surfactant SDS mixture. *Langmuir* **2012**, *28*, 10348–10362.
- (38) Messaoud, G. B.; Promeneur, L.; Brennich, M.; Roelants, S. L.; Le Griel, P.; Baccile, N. Complex coacervation of natural sophorolipid bolaamphiphile micelles with cationic polyelectrolytes. *Green Chem.* **2018**, *20*, 3371–3385.
- (39) Guillemet, F.; Piculell, L. Interactions in aqueous mixtures of hydrophobically modified polyelectrolyte and oppositely charged surfactant. Mixed micelle formation and associative phase separation. *J. Phys. Chem.* **1995**, *99*, 9201–9209.
- (40) Svensson, A.; Piculell, L.; Cabane, B.; Ilekti, P. A new approach to the phase behavior of oppositely charged polymers and surfactants. *J. Phys. Chem. B* **2002**. *106*. 1013—1018.
- (41) Li, Y.; Dubin, P. L.; Havel, H. A.; Edwards, S. L.; Dautzenberg, H. Complex formation between polyelectrolyte and oppositely charged mixed micelles: soluble complexes vs coacervation. *Langmuir* 1995, 11, 2486–2492.
- (42) Pandav, G.; Pryamitsyn, V.; Errington, J.; Ganesan, V. Multibody Interactions, Phase Behavior, and Clustering in Nanoparticle—Polyelectrolyte Mixtures. *J. Phys. Chem. B* **2015**, *119*, 14536–14550.
- (43) Samanta, R.; Halabe, A.; Ganesan, V. Influence of charge regulation and charge heterogeneity on complexation between polyelectrolytes and proteins. *J. Phys. Chem. B* **2020**, *124*, 4421–4435.
- (44) Samanta, R.; Ganesan, V. Direct Simulations of Phase Behavior of Mixtures of Oppositely Charged Proteins/Nanoparticles and Polyelectrolytes. *J. Phys. Chem. B* **2020**, *124*, 10943–10951.
- (45) Samanta, R.; Ganesan, V. Influence of protein charge patches on the structure of protein—polyelectrolyte complexes. *Soft Matter* **2018**, *14*, 9475—9488.
- (46) Pryamitsyn, V.; Ganesan, V. Interplay between depletion and electrostatic interactions in polyelectrolyte—nanoparticle systems. *Macromolecules* **2014**, *47*, 6095—6112.
- (47) Kayitmazer, A. B.; Bohidar, H. B.; Mattison, K. W.; Bose, A.; Sarkar, J.; Hashidzume, A.; Russo, P. S.; Jaeger, W.; Dubin, P. L. Mesophase separation and probe dynamics in protein-polyelectrolyte coacervates. *Soft Matter* **2007**, *3*, 1064–1076.
- (48) Antonov, M.; Mazzawi, M.; Dubin, P. L. Entering and Exiting the Protein-Polyelectrolyte Coacervate Phase via Nonmonotonic Salt Dependence of Critical Conditions. *Biomacromolecules* **2010**, *11*, 51–59.
- (49) Obermeyer, A. C.; Mills, C. E.; Dong, X.-H.; Flores, R. J.; Olsen, B. D. Complex coacervation of supercharged proteins with polyelectrolytes. *Soft Matter* **2016**, *12*, 3570–3581.
- (50) Comert, F.; Dubin, P. L. Liquid-liquid and liquid-solid phase separation in protein-polyelectrolyte systems. *Adv. Colloid Interface Sci.* **2017**, 239, 213–217.
- (51) Zervoudis, N. A.; Obermeyer, A. C. The effects of protein charge patterning on complex coacervation. *Soft Matter* **2021**, *17*, 6637–6645.
- (52) Dubin, P. L.; Curran, M. E.; Hua, J. Critical linear charge density for binding of a weak polycation to an anionic/nonionic mixed micelle. *Langmuir* **1990**, *6*, 707–709.
- (53) Kizilay, E.; Kayitmazer, A. B.; Dubin, P. L. Complexation and coacervation of polyelectrolytes with oppositely charged colloids. *Advances in colloid and interface science* **2011**, *167*, 24–37.
- (54) Perry, S. L.; Li, Y.; Priftis, D.; Leon, L.; Tirrell, M. The effect of salt on the complex coacervation of vinyl polyelectrolytes. *Polymers* **2014**, *6*, 1756–1772.
- (55) Priftis, D.; Xia, X.; Margossian, K. O.; Perry, S. L.; Leon, L.; Qin, J.; de Pablo, J. J.; Tirrell, M. Ternary, tunable polyelectrolyte complex fluids driven by complex coacervation. *Macromolecules* **2014**, *47*, 3076—3085
- (56) Lee, J.; Popov, Y. O.; Fredrickson, G. H. Complex coacervation: A field theoretic simulation study of polyelectrolyte complexation. *J. Chem. Phys.* **2008**, *128*, 224908.

- (57) Sing, C. E. Development of the modern theory of polymeric complex coacervation. *Advances in colloid and interface science* **2017**, 239, 2–16.
- (58) Lytle, T. K.; Sing, C. E. Transfer matrix theory of polymer complex coacervation. *Soft Matter* **2017**, *13*, 7001–7012.
- (59) Perry, S. L.; Sing, C. E. Prism-based theory of complex coacervation: Excluded volume versus chain correlation. *Macromolecules* **2015**, *48*, 5040–5053.
- (60) Adhikari, S.; Leaf, M. A.; Muthukumar, M. Polyelectrolyte complex coacervation by electrostatic dipolar interactions. *J. Chem. Phys.* **2018**, *149*, 163308.
- (61) Zhang, P.; Shen, K.; Alsaifi, N. M.; Wang, Z.-G. Salt partitioning in complex coacervation of symmetric polyelectrolytes. *Macromolecules* **2018**, *51*, 5586–5593.
- (62) Borue, V. Y.; Erukhimovich, I. Y. A statistical theory of globular polyelectrolyte complexes. *Macromolecules* **1990**, 23, 3625–3632.
- (63) Li, L.; Srivastava, S.; Andreev, M.; Marciel, A. B.; de Pablo, J. J.; Tirrell, M. V. Phase behavior and salt partitioning in polyelectrolyte complex coacervates. *Macromolecules* **2018**, *51*, 2988–2995.
- (64) Sing, C.; Perry, S. Recent progress in the science of complex coacervation. *Soft Matter* **2020**, *16*, 2885.
- (65) Salehi, A.; Larson, R. G. A Molecular Thermodynamic Model of Complexation in Mixtures of Oppositely Charged Polyelectrolytes with Explicit Account of Charge Association/Dissociation. *Macromolecules* **2016**, *49*, 9706–9719.
- (66) Friedowitz, S.; Salehi, A.; Larson, R. G.; Qin, J. Role of electrostatic correlations in polyelectrolyte charge association. *J. Chem. Phys.* **2018**, *149*, 163335.
- (67) Lou, J.; Friedowitz, S.; Qin, J.; Xia, Y. Tunable coacervation of well-defined homologous polyanions and polycations by local polarity. *ACS Cent. Sci.* **2019**, *5*, 549–557.
- (68) Qin, J.; de Pablo, J. J. Criticality and connectivity in macromolecular charge complexation. *Macromolecules* **2016**, 49, 8789–8800.
- (69) Priftis, D.; Tirrell, M. Phase behaviour and complex coacervation of aqueous polypeptide solutions. *Soft Matter* **2012**, *8*, 9396–9405.
- (70) Danielsen, S. P. O.; McCarty, J.; Shea, J.-E.; Delaney, K. T.; Fredrickson, G. H. Molecular design of self-coacervation phenomena in block polyampholytes. *Proc. Natl. Acad. Sci. U. S. A.* **2019**, *116*, 8224–8232.
- (71) Delaney, K. T.; Fredrickson, G. H. Theory of polyelectrolyte complexation Complex coacervates are self-coacervates. *J. Chem. Phys.* **2017**, *146*, 224902.
- (72) Marciel, A. B.; Srivastava, S.; Tirrell, M. V. Structure and rheology of polyelectrolyte complex coacervates. *Soft Matter* **2018**, *14*, 2454.
- (73) Srivastava, S.; Andreev, M.; Levi, A. E.; Goldfeld, D. J.; Mao, J.; Heller, W. T.; Prabhu, V. M.; de Pablo, J. J.; Tirrell, M. V. Gel phase formation in dilute triblock copolyelectrolyte complexes. *Nat. Commun.* **2017**, *8*, 14131.
- (74) Van der Gucht, J.; Spruijt, E.; Lemmers, M.; Cohen Stuart, M. A. Polyelectrolyte complexes: Bulk phases and colloidal systems. *J. Colloid Interface Sci.* **2011**, 361, 407–422.
- (75) Huang, J.; Morin, F.; Laaser, J. E. Charge-Density-Dominated Phase Behavior and Viscoelasticity of Polyelectrolyte Complex Coacervates. *Macromolecules* **2019**, *52*, 4957–4967.
- (76) Liu, Y.; Santa Chalarca, C.; Carmean, R.; Olson, R.; Madinya, J.; Sumerlin, B.; Sing, C.; Emrick, T.; Perry, S. Effect of polymer chemistry on the linear viscoelasticity of complex coacervates. *Macromolecules* **2020**, *53*, 7851–7864.
- (77) Manning, G. S. Limiting laws and counterion condensation in polyelectrolyte solutions I. Colligative properties. *J. Chem. Phys.* **1969**, *51*, 924–933.
- (78) Ou, Z.; Muthukumar, M. Entropy and enthalpy of polyelectrolyte complexation: Langevin dynamics simulations. *J. Chem. Phys.* **2006**, 124, 154902.
- (79) Chang, L.-W.; Lytle, T. K.; Radhakrishna, M.; Madinya, J. J.; Vélez, J.; Sing, C. E.; Perry, S. L. Sequence and entropy-based control of complex coacervates. *Nat. Commun.* **2017**, *8*, 1–8.

Macromolecules Article pubs.acs.org/Macromolecules

- (80) Madinya, J. J.; Chang, L.-W.; Perry, S. L.; Sing, C. E. Sequencedependent self-coacervation in high charge-density polyampholytes. Molecular Systems Design & Engineering 2020, 5, 632-644.
- (81) Kudlay, A.; Ermoshkin, A. V.; Olvera de La Cruz, M. Complexation of oppositely charged polyelectrolytes: effect of ion pair formation. Macromolecules 2004, 37, 9231-9241.
- (82) Kudlay, A.; Olvera de la Cruz, M. Precipitation of oppositely charged polyelectrolytes in salt solutions. J. Chem. Phys. 2004, 120,
- (83) Castelnovo, M.; Joanny, J.-F. Complexation between oppositely charged polyelectrolytes: Beyond the Random Phase Approximation. Eur. Phys. J. E 2001, 6, 377-386.
- (84) Kayitmazer, A. B. Thermodynamics of complex coacervation. Advances in colloid and interface science 2017, 239, 169-177.
- (85) Kumar, A.; Dubin, P. L.; Hernon, M. J.; Li, Y.; Jaeger, W. Temperature-Dependent Phase Behavior of Polyelectrolyte- Mixed Micelle Systems. J. Phys. Chem. B 2007, 111, 8468-8476.
- (86) Wang, Y.; Kimura, K.; Dubin, P. L.; Jaeger, W. Polyelectrolytemicelle coacervation: Effects of micelle surface charge density, polymer molecular weight, and polymer/surfactant ratio. Macromolecules 2000, 33, 3324-3331.
- (87) Rathee, V. S.; Sidky, H.; Sikora, B. J.; Whitmer, J. K. Role of associative charging in the entropy-energy balance of polyelectrolyte complexes. J. Am. Chem. Soc. 2018, 140, 15319-15328.
- (88) Neitzel, A. E.; Fang, Y. N.; Yu, B.; Rumyantsev, A. M.; de Pablo, J. J.; Tirrell, M. V. Polyelectrolyte complex coacervation across a broad range of charge densities. Macromolecules 2021, 54, 6878-6890.
- (89) Lytle, T. K.; Sing, C. E. Tuning chain interaction entropy in complex coacervation using polymer stiffness, architecture, and salt valency. Molecular Systems Design & Engineering 2018, 3, 183-196.
- (90) Lytle, T. K.; Chang, L.-W.; Markiewicz, N.; Perry, S. L.; Sing, C. E. Designing electrostatic interactions via polyelectrolyte monomer sequence. ACS central science 2019, 5, 709-718.
- (91) Lytle, T. K.; Salazar, A. J.; Sing, C. E. Interfacial properties of polymeric complex coacervates from simulation and theory. J. Chem. Phys. 2018, 149, 163315.
- (92) Knoerdel, A. R.; Blocher McTigue, W. C.; Sing, C. E. Transfer matrix model of pH effects in polymeric complex coacervation. J. Phys. Chem. B 2021, 125, 8965-8980.
- (93) Svensson, A.; Norrman, J.; Piculell, L. Phase behavior of polyionsurfactant ion complex salts: Effects of surfactant chain length and polyion length. J. Phys. Chem. B 2006, 110, 10332-10340.
- (94) Thalberg, K.; Lindman, B.; Karlstroem, G. Phase behavior of systems of cationic surfactant and anionic polyelectrolyte: influence of surfactant chain length and polyelectrolyte molecular weight. J. Phys. Chem. 1991, 95, 3370-3376.
- (95) Wallin, T.; Linse, P. Monte Carlo simulations of polyelectrolytes at charged micelles. 3. Effects of surfactant tail length. J. Phys. Chem. B 1997, 101, 5506-5513.
- (96) Liu, J.; Takisawa, N.; Shirahama, K.; Abe, H.; Sakamoto, K. Effect of Polymer Size on the Polyelectrolyte- Surfactant Interaction. J. Phys. Chem. B 1997, 101, 7520-7523.
- (97) Singh, S. K.; Nilsson, S. Thermodynamics of interaction between some cellulose ethers and SDS by titration microcalorimetry: II. Effect of polymer hydrophobicity. J. Colloid Interface Sci. 1999, 213, 152–159.
- (98) Zhou, S.; Burger, C.; Yeh, F.; Chu, B. Charge density effect of polyelectrolyte chains on the nanostructures of polyelectrolytesurfactant complexes. Macromolecules 1998, 31, 8157-8163.
- (99) Wang, C.; Tam, K. Interaction between polyelectrolyte and oppositely charged surfactant: effect of charge density. J. Phys. Chem. B 2004, 108, 8976-8982.
- (100) Jonsson, M.; Linse, P. Polyelectrolyte-macroion complexation. I. Effect of linear charge density, chain length, and macroion charge. J. Chem. Phys. 2001, 115, 3406-3418.
- (101) Sing, C. E. Micro- to macro-phase separation transition in sequence-defined coacervates. J. Chem. Phys. 2020, 152, 024902.
- (102) Moreira, A. G.; Netz, R. R. Binding of similarly charged plates with counterions only. *Physical review letters* **2001**, 87, 078301.

- (103) Netz, R. R. Electrostatistics of counter-ions at and between planar charged walls: From Poisson-Boltzmann to the strong-coupling theory. Eur. Phys. J. E 2001, 5, 557-574.
- (104) Koski, J.; Chao, H.; Riggleman, R. A. Field theoretic simulations of polymer nanocomposites. J. Chem. Phys. 2013, 139, 244911.
- (105) Fredrickson, G.; et al. The Equilibrium Theory of Inhomogeneous Polymers; Oxford University Press: 2006; Vol. 134.
- (106) Hooper, J. B.; Schweizer, K. S. Contact aggregation, bridging, and steric stabilization in dense polymer-particle mixtures. Macromolecules 2005, 38, 8858-8869.
- (107) Lauw, Y.; Leermakers, F. A. M.; Cohen Stuart, M. Persistence Length of Wormlike Micelles Composed of Ionic Surfactants: Self-Consistent-Field Predictions. J. Phys. Chem. B 2007, 111, 8158-8168. (108) Doi, M.; Edwards, S. F. The Theory of Polymer Dynamics; Oxford
- University Press: 1988; Vol. 73. (109) Carnahan, N. F.; Starling, K. E. Equation of State for Nonattracting Rigid Spheres. J. Chem. Phys. 1969, 51, 635-636.
- (110) Johnston, B. M.; Johnston, C. W.; Letteri, R. A.; Lytle, T. K.; Sing, C. E.; Emrick, T.; Perry, S. L. The effect of comb architecture on complex coacervation. Organic & biomolecular chemistry 2017, 15, 7630-7642.
- (111) Spruijt, E.; Westphal, A. H.; Borst, J. W.; Cohen Stuart, M. A.; van der Gucht, J. Binodal compositions of polyelectrolyte complexes. Macromolecules 2010, 43, 6476-6484.
- (112) Radhakrishna, M.; Basu, K.; Liu, Y.; Shamsi, R.; Perry, S. L.; Sing, C. E. Molecular connectivity and correlation effects on polymer coacervation. Macromolecules 2017, 50, 3030-3037.
- (113) Wang, X.; Wang, J.; Wang, Y.; Yan, H. Salt effect on the complex formation between cationic gemini surfactant and anionic polyelectrolyte in aqueous solution. Langmuir 2004, 20, 9014-9018.

□ Recommended by ACS

Surface Charge Density and Steric Repulsion in Polyelectrolyte-Surfactant Coacervation

Jason J. Madinya, Sarah L. Perry, et al.

MAY 30, 2023

MACROMOLECULES

READ 2

Effect of Changing Interfacial Tension on Fragmentation Kinetics of Block Copolymer Micelles

Supriya Gupta and Timothy P. Lodge

FEBRUARY 22, 2023

MACROMOLECULES

READ **C**

Modeling Micellar Growth and Branching in Mixtures of **Zwitterionic with Ionic Surfactants**

Alexey I. Victorov, Olga E. Philippova, et al.

SEPTEMBER 19, 2022

LANGMUIR

READ **C**

Salt Counterion Valency Controls the Ionization and Morphology of Weak Polyelectrolyte Miktoarm Stars

Lucie Nová and Filip Uhlík

JULY 06, 2022

MACROMOLECULES

READ 2

Get More Suggestions >